**Estuarine, Coastal and Shelf Science**
September 2022, Volume 275, Pages 107950 (13p.)
https://doi.org/10.1016/j.ecss.2022.107950
https://archimer.ifremer.fr/doc/00779/89075/



# Spatio-temporal dynamics and biogeochemical properties of green seawater discolorations caused by the marine dinoflagellate *Lepidodinium chlorophorum* along southern Brittany coast

Roux Pauline [1], Siano Raffaele [2], Souchu Philippe [1], Collin Karine [1], Schmitt Anne [1], Manach Soazig [1], Retho Michael [3], Pierre Duplessix Olivier [1], Marchand Laetitia [3], Colliec-Jouault Sylvia [3], Pochic Victor [4], Zoffoli Maria Laura [4], Gernez Pierre [4], Schapira Mathilde [1, *]

[1] Ifremer, LITTORAL, F-44300, Nantes, France
[2] Ifremer, DYNECO, F-29280, Plouzané, France
[3] Ifremer, BRM, F-44300, Nantes, France
[4] Nantes Université, Institut des Substances et Organismes de la Mer, ISOMer, UR 2160, F-44000, Nantes, France

* Corresponding author : Mathilde Schapira, email address : mathilde.schapira@ifremer.fr

**Abstract :**

Blooms of the marine dinoflagellate Lepidodinium chlorophorum cause green seawater discolorations affecting the recreational use and the tourism economy along southern Brittany (NE-Atlantic, France). Hypoxic conditions associated with phytoplankton biomass recycling are suspected to cause fauna mortalities. An in situ monitoring was performed in 2019 to characterise the seasonal variability of L. chlorophorum. This species was observed from May to November, with a maximum abundance in June–July. Specific bloom sampling demonstrated a dominance of L. chlorophorum within microphytoplankton, and documented its vertical distribution. Satellite observation was used to compute the surface extent of the bloom and to highlight the importance of small-scale temporal variability, with tidal currents being a primary driver of surface distribution of the bloom. Stratification contributed to promoting the bloom of L. chlorophorum. High concentrations of phosphate and ammonium, together with transparent exopolymer particles (TEP), were recorded within the bloom. Bacterial stimulation, leading to nutrient remineralisation or mucus facilitating mixotrophy, is suggested to sustain bloom development. Hence, TEP production might provide an ecological advantage for the dinoflagellate, conversely causing negative effects on the environment and biological resources through hypoxia. These first insights constitute a baseline for further studies in other ecosystems impacted by this species.

**Highlights**

► *Lepidodinium chlorophorum* occurred from May to November in southern Brittany. ► Water column stratification could favour *L. chlorophorum* blooms. ► High-resolution (5 days, 20 m) satellite observation made possible to document the bloom surface extent and to highlight the influence of tides on the spatial distribution of *L. chlorophorum.* ► High transparent exopolymer particles (TEP) concentrations are measured inside a bloom. Bacterial remineralisation might sustain bloom development for more than one month and cause hypoxia, likely contributing to bivalve mortality.

**Keywords** : Lepidodinium chlorophorum, Coastal waters, HABs, TEP, Hypoxia, Remote sensing

## 1. Introduction

Phytoplankton blooms in marine coastal ecosystems can lead to the accumulation of a high biomass of photosynthetic microorganisms (protists and cyanobacteria; Cloern, 1996). These accumulations often occur at the land-sea interface when the cellular positive net growth surpasses biomass losses, resulting

from the interplay of biological and physical environmental parameters. In coastal systems, phytoplankton blooms are controlled by physico-chemical factors, such as inputs from river flow (Peierls et al., 2012; Hall et al., 2013), coastal upwelling (Brown and Ozretich, 2009), atmospheric deposition (Paerl, 1997), wind (Iverson et al., 1974; Carstensen et al., 2005), nutrient availability (Margalef, 1978), tidal mixing and stratification (Cloern, 1996), heat waves that set up thermal stratification (Cloern et al., 2005), increasing residence time of water (Odebrecht et al., 2015), seasonal changes in temperature, and solar irradiance (Shikata et al., 2008), and biological variables, such as benthic and planktonic grazing pressure (Carstensen et al., 2007; Cloern et al., 2007; Petersen et al., 2008), parasites (Siano et al., 2011; Garvetto et al., 2018), and viral infections (Suttle, 2007).

When occurring at a high biomass, these natural phenomena may cause surface seawater discoloration (i.e., green, red, brown) and/or foam production, thus altering the appearance of coastal waters (Siano et al., 2020) and can have significant impacts on ecosystem functions and services. By altering the aesthetic quality of the coastal areas, seawater discolorations have a negative effect on tourism (Zingone and Enevoldsen, 2000), and the remineralisation of the high volume of biomass produced during intense blooms may create hypoxic/anoxic conditions that are deleterious for marine aquaculture (Sournia et al., 1992). The increase in the distribution and severity of these events may be driven by climate change (Hallegraeff, 2010; Gobler et al., 2017). However, a better understanding of the dynamics and consequences of water discolorations in coastal areas is still needed.

Seawater discoloration in marine coastal waters is produced by different photosynthetic protists and cyanobacteria. Depending on phytoplankton abundances and light intensity, different shades of red discolorations may be induced by the

development of various dinoflagellates (e.g., *Noctiluca scintillans*; Quevedo et al., 1999; Cabal et al., 2008; Zhang et al., 2020) and ciliates (e.g., *Mesodinium rubrum*; Zhang et al., 2020). While dark brown discolorations caused by diatoms are frequently reported worldwide, other phytoplankton species of the phylum Ochrophyta (Heterokontophyta) could also be responsible for dark brown discolorations, including members of the class Raphidophyta and Dictyochophyta (Siano et al., 2020). Green-pigmented microalgal classes (Prasinophyta and Cyanophyta) are known to frequently cause green blooms. The capacity of the marine dinoflagellate *Lepidodinium chlorophorum* to form green seawater discoloration is due to the presence of a green plastid containing chlorophyll *b* (Matsumoto et al., 2011) inherited from a secondary endosymbiosis with a chlorophyte (Kamikawa et al., 2015; Gavalás-Olea et al., 2016; Jackson et al., 2018). Blooms of this unarmoured dinoflagellate (Elbrächter and Schnepf, 1996; Hansen et al., 2007) have been observed in coastal waters worldwide, including Chile (Iriarte et al., 2005; Rodríguez-Benito et al., 2020), California, USA (Gárate-Lizárraga et al., 2014), Australia (McCarthy, 2013), and Europe (Honsell and Talarico, 2004; Sourisseau et al., 2016). Green seawater discolorations due to the massive development of *L*. *chlorophorum* have been frequently reported in southern Brittany since 1982 (Sournia et al., 1992; Siano et al., 2020).

Although the occurrence of *L*. *chlorophorum* is relatively well documented (Honsell et al., 1988; Sournia et al., 1992; Paulmier et al., 1995; Elbrächter and Schnepf, 1996; Sourisseau et al., 2016; Karasiewicz et al., 2020; Siano et al., 2020; Serre-Fredj et al., 2021), the biological and ecological properties that make this species successful in the environment have not yet been fully elucidated. Blooms of this dinoflagellate, which are mainly observed during summer (Belin et al., 2021; Siano et al., 2020), could be supported by the recycling of organic nitrogen in its ammonium

form (Sourisseau et al., 2016). This eurythermal and euryhaline dinoflagellate (Elbrächter and Schnepf, 1996; Claquin et al., 2008) has been observed in river plumes (Sournia et al., 1992; Sourisseau et al., 2016), and the highest densities have been reported occasionally at the pycnocline in stratified waters (Sourisseau et al., 2016). In 2010, high densities of this species (> $10^6$ cells $L^{-1}$) were observed across the Loire River plume (Sourisseau et al., 2016). Furthermore, several studies suggested that *L*. *chlorophorum* could be considered mixotrophic (Hansen and Moestrup, 2005; Jeong et al., 2010; Sourisseau et al., 2016; Ng et al., 2017). The mixotrophic or pure autotrophic characteristic may have strong implications for understanding bloom dynamics. However, while a strain of *Lepidodinium* sp., isolated recently from subtropical coastal waters, has been shown to be a facultative mixotroph (Liu et al., 2021), to our knowledge, the mixotrophy by *L*. *chlorophorum* off Brittany has not yet been clearly established. Moreover, the life cycle of *L*. *chlorophorum* has rarely been studied so far. Benthic cyst production has not been observed, and despite some observations in culture (Sournia et al., 1992), the existence of temporary cysts in the field remains unclear.

*Lepidodinium chlorophorum* is not known to produce toxigenic substances for human or marine fauna, but under non-limiting culture conditions, it excretes a large amount of transparent exopolymer particles (TEP; Claquin et al., 2008; Roux et al., 2021) which may impact marine fauna. TEP are composed of a large amount of carbon, and their aggregations tend to accelerate organic matter sedimentation (Passow et al., 2001; Mari et al., 2017; Bittar et al., 2018). Blooms of *L*. *chlorophorum* have been associated with mass mortalities of fish and cultivated bivalves along the Atlantic French coast (Sournia et al., 1992; Chapelle et al., 1994; Siano et al., 2020), and numerical models have suggested that oysters *(i.e. Crassostrea gigas)* may be

negatively affected when feeding upon *L*. *chlorophorum* (Alunno-Bruscia et al., 2011; Thomas et al., 2016). Even though the direct effect of TEP produced by *L*. *chlorophorum* on marine fauna remains to be elucidated, post-bloom hypoxic/anoxic conditions associated with the recycling of high biomass (phytoplankton cells and TEP) are suspected to be a major cause of fauna mortalities (Sournia et al., 1992; Siano et al., 2020). However, to our knowledge, no study has investigated whether the high production of TEP *in situ* may provide a negative impact and/or an ecological advantage for *L*. *chlorophorum*.

This study aimed to describe seasonal variation of *L*. *chlorophorum* as well as to document bloom biogeochemical properties in the Vilaine Bay (NE Atlantic, France), a coastal area regularly impacted by eutrophication and subsequent algal proliferation (Ratmaya et al., 2019). A specific monitoring field campaign was performed in 2019 to characterise the seasonal variation of this species. To further investigate green seawater discoloration dynamics, high-resolution satellite data were combined with *in situ* sampling during a bloom event in July 2019. The concentration and composition of extracellular polymeric substances produced during *L*. *chlorophorum* bloom were characterised and compared with a recent culture study (Roux et al., 2021). Finally, the potential contribution of TEP produced by *L*. *chlorophorum* on the organic carbon pool was investigated to further assess the potential effects of this biological property of *L*. *chlorophorum* on ecosystem functioning.

## 2. Materials and Methods

### *2.1. Study area*

South Brittany has been identified as a hot spot for *L*. *chlorophorum* bloom development in France (Belin et al., 2021), therefore abundance was analysed in two

bays of this coast: Quiberon and Vilaine (Fig. 1). These bays were selected based on the recurrent observations of this species within the phytoplankton community (Belin et al., 2021; Siano et al., 2020).

Quiberon Bay is a shallow bay (15 m) characterised by weak tidal currents and receive indirect freshwater inputs, as the Loire and Vilaine River plumes tend to spread toward the NW and remain confined along the coast, particularly during early spring (Lazure and Jégou, 1998). Low freshwater inputs combined with low vertical mixing cause strong haline stratification in this bay (Planque et al., 2004). From spring to mid-September, thermal stratification is superimposed onto the haline stratification. During thermal stratification, W/NW winds may induce local upwelling (Lazure and Jégou, 1998; Puillat et al., 2004, 2006).

Vilaine Bay is a 69 $km^2$ shallow bay (10 m) directly influenced by the Vilaine and Loire Rivers, with a mean annual flow of 70 and 850 $m^3 s^{-1}$, respectively (Lazure et al., 2009). The Loire River plume generally spreads NW with a dilution of 20- to 100-fold by the time it reaches the Vilaine (Ménesguen and Dussauze, 2015; Ménesguen et al., 2018). The Vilaine River plume generally spreads throughout the bay before moving westward (Chapelle et al., 1994). A dam located 8 km from the mouth regulate freshwater discharge and was constructed in 1970 to prevent saltwater intrusion upstream (Traini et al., 2015). The Vilaine Estuary is the most sheltered estuary of the French Atlantic coast; the water residence time in the bay varies from 10–20 days depending on the season and is generally longer during calm periods (Chapelle et al., 1994). The water circulation is characterized by low tidal and residual currents and is mainly driven by tide, wind, and river flow (Lazure and Salomon, 1991; Lazure and Jégou, 1998). Haline stratification is strong from February to June in response to high river runoff and relatively low vertical mixing, whereas thermal stratification occurs

between May and mid-September (Puillat et al., 2004). The Vilaine Bay has undergone eutrophication for several decades mainly due to the high nutrient inputs from the Vilaine and Loire Rivers (Rossignol-Strick, 1985; Ratmaya et al., 2019).

### *2.2. Seasonal monitoring in 2019*

To determine the timing for *L. chlorophorum* bloom occurrence, monitoring was performed in Quiberon and Vilaine bays from May to December 2019. Sampling was conducted fortnightly at different day times, but according to high tide (± 2 h), at three stations: Men er Roue (Quiberon Bay), Ouest Loscolo, and Nord Dumet (Vilaine Bay; Fig. 1). Vertical profiles of seawater temperature (°C), salinity, turbidity (nephelometric turbidity unit; NTU), and *in vivo* fluorescence (fluorescein fluorescence unit; FFU) were performed with a multi-parameter probe (NKE MP6) from the subsurface to the water-sediment interface (8–14 m, depending on stations). Water samples were collected using a 5 L Niskin bottle at three depths: subsurface (0–1 m), 1 m above the water-sediment interface and at the fluorescence maximum (Fmax) when present. Water sample aliquots were processed for microphytoplankton identification and enumeration and for chlorophyll *a* concentration ([Chl*a*]; µg $L^{-1}$). Dissolved inorganic nitrogen, phosphorus and silicates concentration ([DIN, DIP, DSi]; µM) were measured as well as TEP ([TEP]; µg Xeq $L^{-1}$) and particulate organic carbon concentration ([POC]; µM). Analytical procedures are described in section 2.4. At the Nord Dumet station, these data were collected every fortnight, in addition to temperature, salinity, and dissolved oxygen concentrations, which were acquired continuously and autonomously by the MOLIT buoy of the COAST-HF network (Coastal OceAn observing SysTem-High Frequency). This instrumented buoy measured these parameters in 1-h intervals at the subsurface and 1 m above the water-sediment interface (Retho et al., 2020). Data on

the river flow was extracted from the French hydrologic database (http://www.hydro.eaufrance.fr/). Daily wind data were retrieved from the weather station Belle Ile – Le Talus (47°17'39"N; 3°13'05"O) from the Météo-France observation network (https://donneespubliques.meteofrance.fr/).

### *2.3. Specific bloom sampling in summer 2019*

On July 9, 2019, a specific sampling strategy was implemented to investigate the spatial structure and hydrological changes caused by the massive development of *L. chlorophorum*. Along a seaward transect, six stations were sampled at high tide: three stations inside and three stations outside the green seawater discoloration. Sampling was performed as previously described. To further investigate the organic matter produced during a bloom, several additional parameters were measured: concentrations of dissolved organic carbon ([DOC]; µM) and nitrogen ([DON]; µM), and nitrite concentration ([$NO_2$]; µM). Moreover, to investigate the composition of the soluble fraction of the extracellular polymeric substances (soluble extracellular polymers, SEP) present within a bloom of *L. chlorophorum*, a subsurface water sample was collected at St1. To complete the characterisation of this bloom event, satellite data were used to estimate its extent and duration.

### *2.4. Analytical procedure of physicochemical and biological variables*

For inorganic nutrients, 300 mL water samples were pre-filtered through 41 µm pore silk directly from the Niskin bottle. For dissolved silicate (i.e., DSi = $Si(OH)_4^-$) concentrations, water samples were filtered through 0.45 µm acetate cellulose membrane and stored at 4°C until analysis. Water samples for the determination of

dissolved inorganic nitrogen (i.e., DIN = $NO_3^-$ + $NO_2^-$ + $NH_4^+$) and phosphorus (i.e., DIP = $PO_4^{3-}$) were stored directly at -20°C. Samples were analysed using an auto-analyser (Seal analytical AA3) following standard protocols (Aminot and Kérouel, 2007). The limits of quantification (LQ) were 0.4 µM for DSi, 0.5 µM for $NO_3^-$ + $NO_2^-$, and 0.05 µM for DIP, $NH_4^+$, and $NO_2^-$. Measurement uncertainty measurement was 12% for DSi, 10% for $NO_3^-$ + $NO_2^-$, 15% for DIP, and 27% for $NH_4^+$.

Total dissolved nitrogen concentrations ([TDN]) was measured using the persulphate oxidation method (Raimbault et al., 1999; Aminot and Kérouel, 2004) and then analysed in segmented continuous flow on the auto-analyser according to Aminot and Kérouel (2007). [DON] were calculated by the difference between [TDN] and [DIN].

To estimate [POC] in the bloom, 100–250 mL were gently filtered onto combusted GF/F filters (Whatman® Nuclepore™; for 4 h at 450°C) and stored at -20°C until analysis. After removal of carbonates with phosphoric acid, filters were treated using a CHN element analyser (Flash 2000, Thermo Fisher Scientific, Waltham, USA) to measure [POC] and nitrogen ([PON]) concentrations (Aminot and Kérouel, 2004). [DOC] were measured on the filtrates collected in acid washed and pre-combusted glass tubes and stored at -20°C. Analyses were conducted using a TOC meter (Shimadzu TOC-$V_{CSH}$). Measurement uncertainty was 12%.

The extracellular polymeric substances were analysed to: 1) estimate [TEP] in the bloom and 2) characterise the composition of SEP present within a bloom of *L. chlorophorum*. [TEP] was determined using a semi-quantitative method based on the colorimetric determination of the amount of dye complexed with extracellular particles (Claquin et al., 2008, adapted from Passow and Alldredge, 1995) as described in Roux et al. (2021). Briefly, triplicate samples of 50–150 mL were gently filtered through 0.4 µm polycarbonate membrane filters (Whatman® Nuclepore™ Track-Etched

Membrane). Particles retained on the filter were stained with Alcian Blue (Sigma) solution. The filters were soaked in 80% sulphuric acid for 2 h and absorbance read at 787 nm using a spectrophotometer (Shimadzu UV-2600). The TEP concentrations are expressed in µg xanthan equiv $L^{-1}$. To characterise the SEP present within a bloom of *L*. *chlorophorum*, 1 L of subsurface water sample collected at St1, located inside the bloom, was centrifuged (4000 g for 30 minutes at 4°C), and protein and monosaccharide contents were characterised (Roux et al., 2021). To confirm the presence of a sulphated polysaccharide, SEP were analysed by both electrophoresis analysis (PAGE gel) and ATR-FTIR spectroscopy and compared to sulphated polysaccharide standards (galactan sulphate MW 80,000, 7.7% S extracted from *Asparagopsis armata*; dextran sulphate sodium salt MW 50,000, 16.0–19.0% S from Sigma D-8787; dextran sulphate sodium salt MW 500,000, 16.0–19.0% S from Sigma D-6001). The PAGE gel (10% w/v acrylamide) was prepared in 1.5 M Tris HCl buffer at pH 8.8 containing ammonium persulphate (0.05% w/v) and tetramethylethylenediamine (Temed). Polyacrylamide stacking gel (4% w/v acrylamide) was prepared in 0.5 M Tris HCl at pH 6.8, ammonium persulphate (10% w/v), and Temed. Samples (40 µL) were prepared in loading buffer (0.5 M Tris HCl pH 6.8, glycerol, 0.5 M EDTA, 0.5% w/v bromophenol) and then loaded on polymerised acrylamide gels. The gel was fixed for 30 minutes in 12.5% (w/v) trichloroacetic acid and stained for 15 minutes with toluidine blue (triméthylthionine hydrochloride) solution at 1% (w/v acetone 80%) and then bleached for 2 h with acetic acid 1%. The FT-IR spectra of the sample and standards were recorded at room temperature using OPUS software at the absorbance mode from 4000 to 400 $cm^{-1}$ (100 scans) with a resolution of 4 $cm^{-1}$ using a Golden Gate single reflection diamond ATR system in a Brucker IFS-55 spectrometer.

Phytoplankton biomass was estimated through [Chl*a*]. Water samples (500–1000 mL) were filtered through GF/F filters (Whatman®) and stored at -20°C until analysis. Inside the bloom, only 5–50 mL water samples were filtered. Chlorophyll was extracted in 10 mL of 90% acetone in the dark at 4°C for 12 h and analysed by monochromatic spectrophotometry (Aminot and Kérouel, 2004). Microphytoplankton (> 20 µm) abundance and community diversity were assessed using an inverted microscope (Zeiss, Axio Observer). One-litre water samples were fixed with Lugol iodine solution (2% f.c.) and stored in the dark at 4°C. Samples were gently homogenised before settling in 10 mL sub-sample for > 12 h in Hydro-Bios counting chambers (Utermöhl, 1958). Limits of quantification was 100 cells $L^{-1}$. In addition, non-fixed 10 mL sub-samples were observed under light microscopy with the aim of confirming the identification of *L. chlorophorum*. Samples collected inside the bloom were diluted 10 times with filtered seawater (0.2 µm). The relative abundance of the main microphytoplankton genera or species (≥ 3%) that were clearly identifiable by light microscopy (dinoflagellates, diatoms, cryptophyceae) were represented. Other genera of these groups as well as ciliophora, euglenoidea and prymnesiophyceae were pooled into a group named “Other”.

### *2.5. Satellite data and processing*

Previous studies have demonstrated that blooms of *L. chlorophorum* can be detected from satellite remote sensing (Sourisseau et al., 2016; Rodríguez-Benito et al., 2020). Satellite remote sensing can detect phytoplankton in the top layer of the water column, from the surface down to the penetration depth (which roughly corresponds to the Secchi depth). Using *in situ* reflectance measurements, the penetration depth was estimated to vary from 2.6 m in bloom areas where *L.*

294 *chlorophorum* was highly concentrated, to 19 m outside the bloom waters (Lee et al.,
295 2005).

296 In the present study, two types of satellite data were used to study the spatial
297 distribution of *L*. *chlorophorum* during the bloom event in 2019 (see sampling map in
298 the Results section). First, a Landsat-8 (L8) image from 9 July 2019 was selected
299 because it was acquired on the same day as the bloom samples. Although L8 did not
300 offer the optimal spectral resolution to accurately detect phytoplankton blooms, it was
301 still useful to roughly observe patches of high [Chl*a*] at a spatial resolution of 30 m
302 (Caballero et al., 2020). L8 data were processed using the POLYMER atmospheric
303 correction (Steinmetz et al., 2011), and [Chl*a*] was roughly estimated using the OC3
304 algorithm (O'Reilly et al., 1998).

305 Second, satellite images from the Sentinel-2 (S2) mission were used to monitor
306 the bloom's spatial distribution and estimate its surface extent in summer 2019. Due to
307 its high spatial resolution (20 m), revisit time (5 days), and radiometric specifications
308 (10 spectral bands in the visible and near-infrared (NIR) spectral domain), S2 is able
309 to detect phytoplankton blooms in optically complex coastal waters (Caballero et al.,
310 2020). Top-of-atmosphere Level-1C data were downloaded from the Copernicus Open
311 Access Hub and corrected from the atmospheric signal to compute the remote-sensing
312 reflectance ($R_{rs}$). Three distinct methods of atmospheric correction (AC) were used,
313 and the estimation of the bloom's surface area was eventually computed as the
314 average from the three methods. The combination of several AC methods was chosen
315 here to filter out radiometric uncertainties and provide a robust estimation of the bloom
316 extent from satellite data. In complement to Sen2cor, the default AC implemented by
317 the European Space Agency (Main-Knorn et al., 2017), two other common AC methods
318 were used: POLYMER (Steinmetz et al., 2011) and GRS (Harmel et al., 2018).

A visual inspection of the S2 imagery over the study area from May to August 2019 was performed to select all images showing a green discoloration typical of a *L*. *chlorophorum* bloom (Siano et al., 2020). Only images showing a conspicuous colour were selected and further processed. Selected images were mostly cloud free and made it possible to accurately detect the bloom's spatial distribution and to compute its areal extent. Partially cloudy images were not used in quantitative analyses but were still useful to investigate bloom temporal dynamics. Bloom detection was performed using an NIR-to-red band ratio algorithm (Gilerson et al., 2010). The reflectance peak near 700 nm is a well-known feature of Chl*a*-rich waters (Gitelson, 1992), and the ability of the $R_{rs}(705)/R_{rs}(665)$ ratio to detect high concentration of chlorophyll-*a* (typically > 7 µg $L^{-1}$) has been previously demonstrated (Lavigne et al., 2021). Red-edge algorithms are known to perform satisfactorily in coastal turbid waters due to the influence of the Chl*a* absorption band around 675 nm as well as the limited interference of non-algal particles (Gernez et al., 2017, Zeng and Binding, 2019) on the NIR-to-red band-ratio. A radiometric threshold of $R_{rs}(705)/R_{rs}(665) > 1.05$ was used here as a bloom indicator for *L*. *chlorophorum*. This threshold was obtained empirically by comparing each cloud-free S2 image with the $R_{rs}$ spectra of 50 pixels located inside the bloom *vs*. 50 pixels outside the bloom. While a recent satellite study of a massive *L*. *chlorophorum* bloom in southern Chile (Rodríguez-Benito et al., 2020) used a threshold corresponding to $R_{rs}(705)/R_{rs}(665) > 1$, we applied a more conservative threshold to reduce the number of false positives. An additional radiometric criterion was further used to detect *L*. *chlorophorum* using its typical green reflectance peak near 560 nm (Sourisseau et al., 2016). Using the same empirical method, we determined that a threshold of $R_{rs}(560)/R_{rs}(490) > 1.2$ improved the discrimination between bloom and non-bloom areas; the combination of both thresholds allowing to

efficiently detect green seawater discoloration pixels, even among the optically complex waters of the Vilaine estuary. Floating macroalgae was excluded using a radiometric threshold in the NIR (e.g., $R_{rs}(865) < 0.01$, Qi and Hu, 2021). Finally, a geometric mask was applied to remove submerged macroalgae surrounding shallow rocky shores, and mudflats where microphytobenthos biofilms could be visible below clear shallow waters.

### *2.6. Statistical analyses*

The spatial distribution of biological and physicochemical parameters during the bloom event was represented by a section scope using the software Ocean Data View (ODV) 5.3.0 (Schlitzer, 2020). As the number of samples per group of variables was low ($n < 10$), the hypotheses of normal distribution (Shapiro-Wilk test) and homoscedasticity of residuals (Bartlett test) were not verified. The Spearman correlation matrix was calculated for all parameters at the subsurface and water-sediment interface. Statistical analyses were performed using R software 3.6.1 (R Core Team, 2019).

## 3. Results

### *3.1.* Lepidodinium chlorophorum *seasonal variation in 2019*

From May to December 2019 (Fig. 2A-U), *L. chlorophorum* was observed both at subsurface and water-sediment interface at the three sampling stations (Fig. 2S, T, U and Fig. S1). The highest abundances were recorded at the Fmax depth (Table 1)

or at the water-sediment interface. Indeed, the abundance of *L*. *chlorophorum* represented 55% of total biomass at the Fmax depth on July 22 at Nord Dumet (2.6 x $10^5$ cells $L^{-1}$ at 10.5 m; Table 1). At the Ouest Loscolo station, the maximal abundance was measured on July 22 (1.9 x $10^5$ cells $L^{-1}$ at the water-sediment interface; Fig. 2T) and on August 6 at the station Men er Roue (5.0 x $10^5$ cells $L^{-1}$ at 5.6 m; Table 1).

At the Nord Dumet station, data from the MOLIT buoy showed a strong decrease in oxygen concentration on July 27 at the water-sediment interface (2.4 mg $L^{-1}$; Fig. S2A), following high *L*. *chlorophorum* abundance (2.6 x $10^5$ cells $L^{-1}$ at 10.5 m), [Chl*a*] (7.3 µg $L^{-1}$; Fig. 2P), and [POC] (39 µM; Fig. 2M) registered on July 22 at the Nord Dumet station. In addition, an increase in [TEP] was measured at the water-sediment interface between August 6 (1028 µg Xeq $L^{-1}$) and August 20 (2882 µg Xeq $L^{-1}$; Fig. 2J). One month earlier than this bloom (June 7), an increase in the Vilaine River flow was observed (Fig. S3). During this period, the average flow was higher (39 $m^3$ $sec^{-1}$) than the usual summer average (10 $m^3$ $sec^{-1}$), with a maximum of 69 $m^3$ $sec^{-1}$ (Fig. S3). The freshwater input subsequently reached station Nord Dumet, as suggested by the subsurface salinity decrease on June 17 (Fig. 2D and Fig. S2B). Then, water column thermal stratification occurred from June 26 to July 22, with higher temperatures at the subsurface than at the water-sediment interface (Fig. 2A and Fig. S2C).

The freshwater input was also observed at station Ouest Loscolo, as shown by the salinity decrease in June–July (32.0; Fig. 2E) and the subsurface increase in nutrient concentrations ([$NO_3$+$NO_2$] = 5.7 µM; [DIP] = 0.27 µM; [DSi] = 8.8 µM; Fig. S4). This event was followed on July 22 by an increase in the abundance of *L*.

391 *chlorophorum* (1.9 x $10^5$ cells $L^{-1}$; Fig. 2T and Fig. S1D) and [Chl*a*] (8.2 µg $L^{-1}$; Fig. 2Q)
392 at the water-sediment interface.

393 In the bay of Quiberon, the station Men er Roue was less influenced by
394 freshwater inputs than the stations of Vilaine Bay and the salinity remained stable
395 around 34 throughout the summer (Fig. 2F). However, a *L*. *chlorophorum* bloom was
396 observed at the Fmax depth (5.0 x $10^5$ cells $L^{-1}$; Table 1) and at the water-sediment
397 interface (3.1 x $10^4$ cells $L^{-1}$; Fig. 2U and Fig. S1F) on August 6, when a thermocline
398 was recorded.

399

400 ***3.2. Analysis of a water discoloration***

401

402 ***3.2.1. Spatial dynamics of a water discoloration***

403 Green seawater discolorations were conspicuously visible on Sentinel-2 images
404 (Fig. 3) during the studied bloom event. *In situ* measurements performed within the
405 green seawater discoloration (see below) confirmed that the bloom visible on the S2
406 images was dominated by *L. chlorophorum*, at surface concentration > $10^6$ cells $L^{-1}$ in
407 the greenest waters. The high spatial resolution (20 m) of S2 images made possible to
408 study surface distribution over the whole study area, thus usefully complementing
409 station-based monitoring (see 3.1). While satellite monitoring was occasionally
410 hampered by cloud cover, the screening of cloud-free S2 observations suggested that
411 the bloom started around mid-June and had vanished by late July / early August (Table
412 2). The influence of tidal circulation appeared to be a primary driver of the bloom spatial
413 structure: patches of high chlorophyll concentration were transported inside the Vilaine
414 Estuary at high tide (Fig. 3A, B) and moved seaward during ebb (Fig. 3C, D). At low

tide, the bloom was concentrated along a narrow frontal zone outside the estuary (Fig. 3E, F). During the bloom event, the bloom surface area varied from 2.37 to 12.95 $km^2$ with a maximum around late June–early July (Table 2).

*In situ* sampling made it possible to document the composition of the microphytoplankton community within the green seawater discoloration patch on July 9, 2019. Three stations (St1-3) of the radial sampling were located in extremely green waters, as highlighted by both satellite and *in situ* observations (Fig. 3G, H), whereas the remaining sampling stations (St4-6) were located outside the bloom (Fig. 3G). Analyses of the microphytoplankton community composition confirmed that the bloom to a high relative abundance of *L*. *chlorophorum* (Fig. 4). Within the bloom, *L. chlorophorum* represented more than 95% of total microphytoplankton abundance at both sampling depths (Fig. 4). Outside the bloom, *L*. *chlorophorum* was relatively less abundant at the subsurface (relative abundance < 23%, Fig. 4A) than at the water-sediment interface. At St4, while *L*. *chlorophorum* dominated the microphytoplankton community at the water-sediment interface (> 94%; Fig. 4B), other dinoflagellates, such as *Gymnodinium* spp., *Gyrodinium* spp., *Scrippsiella* spp., and *Protoperidinium* spp., dominated at the subsurface (Fig. 4A). From St4 seaward, the proportion of dinoflagellates within the microphytoplankton community tended to decrease, with *Leptocylindrus* spp. the most dominant diatom genus at the subsurface at St6 (Fig. 4A). The diatom genus *Chaetoceros* spp. and the dinoflagellate *Dinophysis* spp. were only detected (≥ 3%) at the water-sediment interface at St6 (Fig. 4B).

Following these changes in the phytoplankton community, both Chl*a* and *L*. *chlorophorum* concentrations sharply declined from nearshore to offshore. The highest phytoplankton biomass was recorded at St1, with [Chl*a*] ranging from 38 μg $L^{-1}$ at the water-sediment interface to 73 μg $L^{-1}$ at the subsurface (Fig. S5A). *Lepidodinium*

*chlorophorum* abundance was up to 2000-fold higher at the subsurface inside (St1) than outside the bloom (St6; Fig. 5A). The highest abundance was recorded at the subsurface at St1 (8.9 x $10^6$ cells $L^{-1}$), and the lowest was observed at the subsurface at St6 (4.1 x $10^3$ cells $L^{-1}$; Fig. 5A). At the water-sediment interface, *L*. *chlorophorum* was observed throughout the sampled area, with values ranging from 3.2 x $10^6$ cells $L^{-1}$ within the bloom (St1) to 53.4 x $10^3$ cells $L^{-1}$ outside the bloom (St6, Fig. 5A).

A decreasing temperature gradient was observed seaward from St1 (19.6 ± 0.9°C) to St6 (18.4 ± 0.8°C) at both sampling depths (Fig. 5B). In contrast, salinity increased seaward, both in subsurface waters (from 32.4 to 34.1) and at the water-sediment interface (from 33.8 to 34.0; Fig. 5C). While [DSi] declined gradually along the salinity gradient from 21 µM at St1 to 13.7 µM at St6 at the subsurface (Fig. 5D), other inorganic nutrient concentrations followed a spatial pattern similar to that observed for *L*. *chlorophorum* abundance. Moreover, the highest [$NO_2$] (Fig. S5B), [$NH_4$] (Fig. 5E), and [DIP] (Fig. 5F) were recorded at the subsurface within the bloom (at St1, [$NO_2$], [$NH_4$], and [DIP] were 0.14, 0.48, and 1.63 µM, respectively). In contrast, [$NO_3$] was very low throughout the sampling area, with values remaining below the limit of quantification (i.e., LQ < 0.5 µM) at the six sampling stations and both depths (Fig. S5C).

### *3.2.2. Biogeochemical characteristics of the water discoloration*

[DON] (Fig. 5G) and [DOC] (Fig. S5D) showed a spatial pattern similar to that of *L*. *chlorophorum* abundance, with a subsurface maximum at St1 (66 and 655 µM, respectively). Subsequently, [DON] and [DOC] decreased sharply seaward, with the lowest values at St6 ([DON] < 12 µM; [DOC] < 200 µM). The DOC/DON ratio was lower inside (St1, subsurface: 9.9; water-sediment interface: 7.4) than outside the bloom

(St6, subsurface: 16.0; water-sediment interface: 13.8; Table S1). In contrast, the POC/PON ratio was higher inside (St1, subsurface: 11.5; water-sediment interface: 11.2) than outside the bloom (St6, subsurface: 7.1; water-sediment interface: 6.7; Table S1). [POC] and [PON] (Fig. S5E, F) followed the same pattern as the dissolved fraction. The highest [POC] and [PON] were measured at the subsurface at St1 (1163 and 101 µM, respectively). The highest [TEP] was recorded at St1, ranging from 3579 at the water-sediment interface to 24446 µg Xeq $L^{-1}$ at the subsurface (Fig. 5H). The [TEP] also dramatically decreased seaward and reached a very low value at St6, with concentrations of 677 and 455 µg Xeq $L^{-1}$ at the water-sediment interface and subsurface, respectively (Fig. 5H). At the subsurface, [TEP] was up to 50-fold higher inside (St1) than outside the bloom (St6).

To establish the carbon signature of an *L*. *chlorophorum* bloom, a conversion factor of 0.51 was used to convert from µg Xeq to µgC (TEP-C; Passow and Engel, 2001). Considering the TEP-C and POC values reported in this study, the TEP-C contribution to the POC pool (TEP-C%POC) was estimated. In subsurface waters, the TEP-C ranged from 3509 to 12468 µg $L^{-1}$ inside the bloom and from 232 to 467 µg $L^{-1}$ outside the bloom. The TEP-C%POC contribution was higher inside (59–89%:St1, St2, St3) than outside (44–61%:St4, St5, St6) the bloom.

The SEP from the St1 supernatant, collected at the subsurface inside the bloom, were mainly composed of proteins and neutral monosaccharides. Both galactose and glucose were predominant over other neutral monosaccharides that were also detected, such as rhamnose and mannose. For electrophoresis gels (Fig. S6), the St1 supernatant presented a similar profile (a polydisperse blot) to galactan sulphate (molecular weight; MW 80000) and dextran sulphate (MW 50000). The absence of a smear in the stacking gel, as observed with dextran sulphate (MW 500000), indicated

that no high molecular weight chains were present in the sample. The SEP molecular weight of St1 was below 100,000. The colour intensity of the St1 supernatant was close to that of galactan sulphate, suggesting a similar sulphur content close to 8%. Moreover, its electrophoretic mobility and profile indicated a similar molecular weight and polydispersity to those of standard galactan sulphate. The ATR-FTIR spectra were characteristic of polysaccharides with a broad absorption band attributed to the O-H stretching vibration above 3000 $cm^{-1}$ and an intense absorption between 1650 and 1050 $cm^{-1}$, corresponding to characteristic bands of polysaccharides (Fig. S7). Moreover, at 2931 $cm^{-1}$, a band assigned to the C-H symmetrical stretching vibration was also present. The presence of sulphate groups was confirmed in all polysaccharides with strong absorption bands at 1230 $cm^{-1}$, which corresponded to the asymmetrical stretching vibration of the sulphate ester groups (S=O), and at 813 and 815 $cm^{-1}$, which was assigned to the C-O-S vibration; these bands were more intense in the highly sulphated dextran sulphate.

### *3.2.3*. *Relationship of* L. chlorophorum *with other biogeochemical parameters*

*Lepidodinium chlorophorum* abundance was positively correlated with [Chl*a*], [DIP], [$NO_2$] and [DON] ($r > 0.90$; $p < 0.05$) at the subsurface (Table S2A). [TEP] was also correlated with cell abundance ($r = 0.94$; $p < 0.05$) and [POC] ($r = 1$; $p < 0.05$) at the subsurface (Table S2A). In contrast, [$NH_4$] was negatively correlated with [Chl*a*] and dinoflagellate abundance ($r = -0.89$; $p < 0.05$) at the water-sediment interface (Table S2B). Overall, *L*. *chlorophorum* concentrations were positively correlated with temperature, concentration of dissolved and particulate organic matter, and [$NH_4$] and [DIP].

## 4. Discussion

The dinoflagellate *L*. *chlorophorum* is an example of a phytoplankton species causing green seawater discolorations worldwide (Honsell and Talarico, 2004; Iriarte et al., 2005; McCarthy, 2013; Gárate-Lizárraga et al., 2014; Rodríguez-Benito et al., 2020). The present study described the seasonal variation of this species in the southern Brittany coast and characterized some biogeochemical properties of a bloom event of this species, for the first time.

### *4.1*. *Physical factors influencing* L. chlorophorum *bloom dynamics*

Our results confirmed that *L*. *chlorophorum* occurs from May to November in South Brittany (Sournia et al., 1992; Sourisseau et al., 2016; Siano et al., 2020). While the environmental parameter variations observed in 2019 are congruent with the main seasonal dynamics generally recorded in the Vilaine and Quiberon bays (Fig. S8), the year 2019 was characterised by a significant increase in the Vilaine River flow during late May - early June (Fig. S3). This intermittent freshwater input and the increase in surface water temperature contributed to the establishment of water column stratification, creating favourable conditions for the development of the bloom. Indeed, the highest *L*. *chlorophorum* concentration and bloom surface extent (Table 2) were recorded in July when the water column was stratified.

Water-mass stratification is considered an essential physical condition that dinoflagellates require to bloom (Margalef, 1978; Smayda, 2002a). Previous studies highlighted the occurrence of high densities of *Alexandrium catenella* (Giacobbe et al., 1996; Anderson et al., 2012; Yamamoto et al., 2013; Condie et al., 2019) and *Dinophysis* sp. (Velo-Suarez et al., 2009; Diaz et al., 2021) in subsurface thin layers,

in correspondence with the pycnocline (Nielsen et al., 1990; Kononen et al., 2003; Lips et al., 2010). In these layers, primary production can exceed surface production (Richardson et al., 2000). For *L*. *chlorophorum*, Sourisseau et al. (2016) observed high densities at the pycnocline in stratified areas. Our study showed that the influence of the Vilaine River and the establishment of thermal stratification affect the development of this species in the water column, corroborating previous studies suggesting that *L*. *chlorophorum* blooms could be correlated with freshwater input from rivers (Sournia et al., 1992; Karasiewicz et al., 2020). These environmental conditions correspond to the Type I habitat (shallow, nutrient-enriched, nearshore waters) described by Smayda (2002b), in which small gymnodinoid species, such as *L*. *chlorophorum*, tend to predominate.

The highest abundances of *L. chlorophorum* were recorded at the Fmax depth or at the water-sediment interface, suggesting that this species could migrate vertically through the water column (Sourisseau et al., 2016). As demonstrated for other dinoflagellates (Dagenais-Bellefeuille and Morse, 2013; Glibert et al., 2016), *L. chlorophorum* could use nutrients located below the pycnocline. Moreover, mixotrophic organisms are able to predate nano-flagellates and bacteria located below the pycnocline. However, to our knowledge, vertical migration as well as mixotrophy have not been clearly established for *L*. *chlorophorum*, but just supposed (Hansen and Moestrup, 2005; Ng et al., 2017; Liu et al., 2021).

As wind speed (< 8 knots; mainly from N to NE sectors), vertical mixing (neap tide period) and Vilaine River flow remained low for more than one month, the bloom event documented in the present study could then be considered an ideal case to study the effects of tidal variations on phytoplankton distribution in a macro tidal estuary. Satellite observations highlighted the influence of short-scale variability on the bloom

surface extent and spatial distribution associated with semi-diurnal tidal dynamics. The location of *L*. *chlorophorum* patches detected by high-resolution remote sensing was consistent with biophysical modelling, where the accumulation of phytoplankton biomass is driven by the interplay between local processes, such as horizontal transport along the main river channel, cross-estuary oscillations, lateral sloshing (Lucas et al., 1999a), and variability in phytoplankton growth rates and population dynamics (Lucas et al., 1999b). Red-edge algorithms are not affected by changes in turbidity associated with river plumes, and the high-resolution Sentinel-2 observations proved useful in estimating the temporal and spatial dynamics of the green seawater discoloration in the first optical layer (i.e. the top 3 m) during summer. However, the detection of relatively high *L. chlorophorum* abundance at the depth of fluorescence maximum and/or below the pycnocline suggest that a significant part of the bloom's biomass may remain undetectable from passive satellite remote sensing.

### *4.2*. *Biogeochemical specificity of* L. chlorophorum *blooms*

The distribution of TEP in marine ecosystems results from the balance between sources, consumption by organisms, and sinks (Alldredge et al., 1998; Passow, 2002). In 2019, the seasonal [TEP] measured in the Vilaine and Quiberon bays were in the highest range of values recorded in coastal seawaters at different locations of the world (Passow, 2002). Higher [TEP] are frequently reported in productive areas or during blooms (Engel, 2004; Corzo et al., 2005; Prieto et al., 2006; Ortega-Retuerta et al., 2009, 2010; Bar-Zeev et al., 2011). For *L*. *chlorophorum*, enrichment experiments on the natural population have shown that [TEP] increased by a factor of 3 in DIP enrichment and by a factor of 1.9 in both DIN and DIN/DSi enrichments (Serre-Fredj et al., 2021). Our study confirmed that a *L*. *chlorophorum* bloom produce a high [TEP]

*in situ*. Moreover, subsurface concentrations of *L*. *chlorophorum* and [TEP] measured inside the bloom were similar to the values obtained by Roux et al. (2021) under laboratory conditions (12 x $10^6$ cells $L^{-1}$ and 17 x $10^3$ µg Xeq $L^{-1}$, respectively). In addition, SEP collected inside the bloom were mainly composed of proteins, glucose and galactose, and the presence of sulphated exopolysaccharides was observed. These results corroborate the SEP composition previously found under laboratory conditions (Roux et al., 2021). Therefore, *L*. *chlorophorum* produce a sulphated exopolysaccharide composed mainly of galactose, confirming that galactose-based exopolysaccharide is a common characteristic among dinoflagellates (Hasui et al., 1995; Yim et al., 2007; Mandal et al., 2011). While sources of TEP and SEP from terrestrial freshwater inputs cannot be completely excluded (Attermeyer et al., 2019), these results reported high TEP concentrations within a bloom and suggest that *L. chlorophorum* is the main responsible for this production.

Subsurface [DIP] and [$NH_4$] were drastically higher inside than outside the bloom. Concentrations recorded on July 8, 2019 at the most upstream station in the Vilaine Estuary (salinity = 32.0) were used to evaluate the origin of these inorganic nutrients (Fig. S9). The behaviour of DSi along the salinity gradient was conservative (Fig. S9A) while those of DIP and $NH_4$ denote a production inside the bloom (Fig. S9B, C). These results suggest that important nutrient recycling occur inside the bloom. This hypothesis is supported by the high subsurface dissolved organic matter concentrations. Indeed, DON may be released by exudation from phytoplankton and bacteria (Bronk and Ward, 1999; Diaz and Raimbault, 2000) or from cell death or viral lysis (Fuhrman, 1999). While allochthonous sources of DON from terrestrial runoff, leaching from plant detritus and soils into streams, rivers, and sediments, and

atmospheric deposition cannot completely be excluded, other parameters tend to support the hypothesis of intense remineralisation processes inside the bloom.

The POC/PON ratio was higher than the Redfield ratio (C/N = 106/16; Redfield, 1958) inside the bloom, suggesting an accumulation of TEP and detrital organic matter produced by *L*. *chlorophorum* in subsurface waters. In contrast, the DOC/DON ratio was lower inside than outside the bloom. These results suggest that organic matter, produced by *L*. *chlorophorum* and maintained in subsurface waters, could provide a microenvironment promoting bacterial development and remineralisation processes (Alldredge and Gotschalkt, 1989; Schapira et al., 2012a, 2012b). Through the microbial loop, bacteria provide regenerated inorganic nutrients (Caron, 1994). Moreover, previous studies suggested that *L*. *chlorophorum* could present high ammonium assimilation rates (Iriarte et al., 2005; Karasiewicz et al., 2020). Presumably, inorganic nutrients regenerated by bacterial remineralisation within the bloom might sustain the development of *L*. *chlorophorum* cells. This could be especially prevalent during calm periods (neap tide and low wind) when the water residence time is longer in the Vilaine Bay (Chapelle et al., 1994). Furthermore, the studied bloom was observed by satellite image for more than one month, confirming bloom duration deduced by citizen observations in this area (Siano et al., 2020). As shown under laboratory conditions (Roux et al., 2021), a strong relationship was suggested between *L*. *chlorophorum* and its associated bacterial consortia through remineralisation processes within a bloom. The bacterial compartment within a bloom remains to be investigated. However, the microenvironment established within a bloom can attract different types of organisms. Previous studies reported that bacteria, protozoa, phytoplankton and metazoan colonize TEP (Simon et al., 2002; Lyons et al., 2007; Shapiro et al., 2014). As the genus *Lepidodinium* is suspected mixotrophic (Hansen and Moestrup, 2005; Ng et al.,

2017; Liu et al., 2021), *L. chlorophorum* could predate also heterotrophic organisms, such as nano-flagellates.

### *4.3. Potential harmful effects of* L. chlorophorum *blooms on the environment*

TEP aggregation tends to accelerate the sedimentation of organic matter from the surface to the seabed (Passow et al., 2001; Mari et al., 2017; Bittar et al., 2018). As demonstrated in a previous study performed under laboratory conditions (Roux et al., 2021), our results confirmed that TEP produced during a bloom of *L. chlorophorum* were associated with high [POC] *in situ*. Moreover, TEP contribute to carbon export and can represent a significant fraction of the carbon pool in our study, as well as others (Passow et al., 2001; Mari et al., 2017; Bittar et al., 2018). In the estuarine system, Annane et al. (2015) showed that TEP-C combined with phytoplankton-C were major contributors to the carbon pool (41 and 54%, respectively) and significantly contributed to the decrease in oxygen concentration in the bottom layer by respiration/remineralisation processes.

Our observations suggested that the large amount of TEP (carbon-rich) excreted by *L. chlorophorum* could enhance remineralisation processes in the water column and accentuate hypoxia close to the water-sediment interface. Oxygen concentrations measured during summer 2019 supported this hypothesis. Indeed, low oxygen concentrations (2.4 mg $L^{-1}$) were recorded at the water-sediment interface by the autonomous buoy located at the Nord Dumet station following an *L. chlorophorum* bloom. These low oxygen concentrations could have extensive consequences for marine fauna. For many benthic invertebrates, the hypoxia threshold is about 2.9 mg $L^{-1}$ or less (Herreid, 1980; Rosenberg et al., 1991; Diaz and Rosenberg, 2008). The

reduction in feeding activity and oxygen consumption is a commonly observed response to hypoxia in bivalves (Sobral and Widdows, 1997; Hicks and McMahon, 2002). However, more data regarding oxygen concentrations at the water-sediment interface are needed to confirm these results. *In situ* and *in vitro* experiments focused on the interaction between *L*. *chlorophorum* and bivalves could complete the analyses on the ecological and potentially harmful impact of this dinoflagellate.

## Conclusions

Coastal blooms of the marine green dinoflagellate *L*. *chlorophorum* can cause summer green seawater discolorations worldwide. Using an original combination of field sampling and high-resolution satellite remote sensing, the present study characterized phytoplankton spatio-temporal distribution and biogeochemical properties during a massive bloom of this dinoflagellate in the bay of Vilaine, an eutrophic estuary of the French Atlantic coast. *Lepidodinium chlorophorum* occurred from May to November, with very high surface abundance during summer (June–July). Occasionally, high abundances of *L*. *chlorophorum* were also recorded at the Fmax depth or deeper. Freshwater inputs (a few weeks before the bloom), sea-surface warming, and thermohaline stratification promoted bloom development. The bloom spatial distribution was then influenced by tidal variability, with seaward and landward movements associated with ebb and flow tide, respectively.

*Lepidodinium chlorophorum* produced a large amount of TEP (carbon-rich). In addition, the SEP produced by this species were mainly composed of sulphated galactan. The high secretion of extracellular polymeric substances, a biological trait particularly developed by this dinoflagellate in comparison to other species, could

686 confer a specific ecological advantage to *L*. *chlorophorum*. The production of TEP
687 would enhance bacteria remineralisation, which would provide nutrients to sustain the
688 bloom for a long period, especially during calm conditions (low wind, and persistent
689 water column stratification). TEP could also facilitate mixotrophy by attracting a large
690 number of heterotrophic organisms. However, the large amount of TEP excreted within
691 the bloom could have a harmful effect on the environment, causing marine fauna and
692 cultivated bivalve mortalities through the enhancement of oxygen reduction, especially
693 close to the water-sediment interface. Further studies are needed to investigate the
694 role of bacteria within the bloom and to fully assess the role of green seawater
695 discoloration on oxygen concentration and potential impact on bivalves. These first
696 insights into the ecological properties of *L. chlorophorum* in southern Brittany constitute
697 the baseline for further studies in other ecosystems impacted by this species.

698

699 **Competing interests**

700 The authors declare that they have no competing interests.

701

702 **Author contributions statement**

703 **Pauline Roux**: Formal analysis, Data curation, Writing original Draft; **Raffaele Siano**:
704 Conceptualization, Writing - Review & Editing; **Philippe Souchu**: Writing - Review &
705 Editing; **Karine Collin**: Investigation, Visualization; **Anne Schmitt**: Investigation,
706 Visualization; **Soazig Manach**: Investigation, Visualization; **Michael Retho**:
707 Investigation, Visualization; **Olivier Pierre-Duplessix**: Investigation, Visualization;

**Laetitia Marchand**: Investigation, Visualization; **Sylvia Colliec-Jouault**: Writing - Review & Editing; **Victor Pochic**: Investigation, Visualization, Writing - Review & Editing; **Maria Laura Zoffoli**: Investigation, Writing - Review & Editing; **Pierre Gernez**: Investigation, Visualization, Writing - Review & Editing; **Mathilde Schapira**: Conceptualization, Methodology, Supervision; Project administration, Funding acquisition. All authors reviewed and accepted the final version of the manuscript.

## Acknowledgements

This work was carried out in the frame of the PhD of PR, financed by Ifremer and Region Pays de la Loire (project LEPIDO-PEN [06582 2019]), and was supported by the Centre National d' Etudes Spatiales (TOSCA projects LASHA and OSYNICO). The authors thank IFREMER-LER/MPL staff for their technical contributions. The authors wish to thank Calypso Bouvier for dedicated assistance in TEP measurements, Elise Robert for particulate organic carbon measurements, and Arnaud Fillaudeau for ATR-FTIR analysis. The authors acknowledge the USGS and the European Space Agency (ESA) for the Landsat-8 and Sentinel-2 observations. We would like to thank Tristan Harmel (Géosciences Environnement Toulouse, GET) and Kien Trung (Laboratoire d'Océanologie et Géosciences, LOG) for the atmospheric correction of satellite data. Pauline Roux, Mathilde Schapira, Raffaele Siano, Karine Collin, Anne Schmitt, Olivier Pierre-Duplessix, Michael Retho, and Soazig Manach are part of GDR PHYCOTOX, a CNRS/IFREMER network on Harmful Algal Blooms (https://www.phycotox.fr/). Finally, the authors thank the anonymous reviewers for their careful reading of our manuscript and their insightful comments and suggestions.

## References


Alldredge, A. L., Gotschalk, C. C., 1989. Direct observations of the mass flocculation of diatom blooms: characteristics, settling velocities and formation of diatom aggregates. Deep-Sea Res. 36(2), 159-171. https://doi.org/10.1016/0198-0149(89)90131-3

Alldredge, A. L., Passow, U., Haddock, S. H. D., 1998. The characteristics and transparent exopolymer particle (TEP) content of marine snow formed from thecate dinoflagellates. J. Plankton Res. 20(3), 393–406. https://doi.org/10.1093/plankt/20.3.393

Alunno-Bruscia, M., Bourlès, Y., Maurer, D., Robert, S., Mazurié, J., Gangnery, A., Goulletquer, P., Pouvreau, S., 2011. A single bio-energetics growth and reproduction model for the oyster *Crassostrea gigas* in six Atlantic ecosystems. J. Sea Res. 66, 340–348. https://doi.org/10.1016/j.seares.2011.07.008

Aminot, A., Kérouel, R., 2004. Hydrologie des écosystèmes marins : paramètres et analyses (in French). Ed. Ifremer, Plouzané, France.

Aminot, A., Kérouel, R., 2007. Dosage automatique des nutriments dans les eaux marines : méthodes en flux continu (in French). Ed. Ifremer, Plouzané, France.

Anderson, D. M., Alpermann, T. J., Cembella, A. D., Collos, Y., Masseret, E., Montresor, M., 2012. The globally distributed genus *Alexandrium*: Multifaceted roles in marine ecosystems and impacts on human health. Harmful Algae. 14, 10–35. https://doi.org/10.1016/j.hal.2011.10.012

Annane, S., St-Amand, L., Starr, M., Pelletier, E., Ferreyra, G. A., 2015. Contribution of transparent exopolymeric particles (TEP) to estuarine particulate organic carbon pool. Mar. Ecol. Prog. Ser. 529, 17–34. https://doi.org/10.3354/meps11294

Attermeyer, K., Andersson, S., Catalán, N., Einarsdottir, K., Groeneveld, M., Székely, A. J., Tranvik, L. J., 2019. Potential terrestrial influence on transparent exopolymer particle concentrations in boreal freshwaters. Limnol. Oceanogr. 64, 2455–2466. https://doi.org/10.1002/lno.11197

Bar-Zeev, E., Berman, T., Rahav, E., Dishon, G., Herut, B., Kress, N., Berman-Frank, I., 2011. Transparent exopolymer particle (TEP) dynamics in the eastern Mediterranean Sea. Mar. Ecol. Prog. Ser. 431, 107–118. https://doi.org/10.3354/meps09110

Belin, C., Soudant, D., Amzil, Z. 2021. Three decades of data on phytoplankton ond phycotoxins on the French coast: Lessons from REPHY and REPHYTOX. Harmful Algae. 101733. https://doi.org/10.1016/j.hal.2019.101733

Bittar, T. B., Passow, U., Hamaraty, L., Bidle, K. D., Harvey, E. L., 2018. An updated method for the calibration of transparent exopolymer particle measurements. Limnol. Oceanogr. Methods. 16, 621-628. https://doi.org/10.1002/lom3.10268

Bronk, D. A., Ward, B. B., 1999. Gross and net nitrogen uptake and DON release in the euphotic zone of Monterey Bay, California. Limnol. Oceanogr. 44(3), 573–585. https://doi.org/10.4319/lo.1999.44.3.0573

Brown, C. A., Ozretich, R. J., 2009. Coupling between the coastal ocean and yaquina bay, oregon: Importance of oceanic inputs relative to other nitrogen sources. Estuaries Coast. 32, 219–237. https://doi.org/10.1007/s12237-008-9128-6

Cabal, J., González-Nuevo, G., Nogueira, E., 2008. Mesozooplankton species distribution in the NW and N Iberian shelf during spring 2004: Relationship with frontal structures. J. Mar. Syst. 72, 282–297. https://doi.org/10.1016/j.jmarsys.2007.05.013

Caballero, I., Fernández, R., Escalante, O. M., Mamán, L., Navarro, G., 2020. New

capabilities of Sentinel-2A/B satellites combined with in situ data for monitoring small harmful algal blooms in complex coastal waters. Sci. Rep. 10, 8743. https://doi.org/10.1038/s41598-020-65600-1

Caron, D. A., 1994. Inorganic Nutrients, Bacteria, and the Microbial Loop. Microb. Ecol. 28(2), 295–298. https://doi.org/10.1007/BF00166820

Carstensen, J., Frohn, L. M., Hasager, C. B., Gustafsson, B. G., 2005. Summer algal blooms in a coastal ecosystem: the role of atmospheric deposition versus entrainment fluxes. Estuar. Coast. Shelf Sci. 62, 595–608. https://doi.org/10.1016/j.ecss.2004.09.026

Carstensen, J., Henriksen, P., Heiskanen, A. S., 2007. Summer algal blooms in shallow estuaries: Definition, mechanisms, and link to eutrophication. Limnol. Oceanogr. 52(1), 370–384. https://doi.org/10.4319/lo.2007.52.1.0370

Chapelle, A., Lazure, P., Ménesguen, A., 1994. Modelling Eutrophication Events in a Coastal Ecosystem. Sensitivity Analysis. Estuar. Coast. Shelf Sci. 39, 529–548. https://doi.org/10.1016/S0272-7714(06)80008-9

Claquin, P., Probert, I., Lefebvre, S., Veron, B., 2008. Effects of temperature on photosynthetic parameters and TEP production in eight species of marine microalgae. Aquat. Microb. Ecol. 51, 1-11. https://doi.org/10.3354/ame01187

Cloern, J. E., 1996. Phytoplankton bloom dynamics in coastal ecosystems: A review with some general lessons from sustained investigation of San Francisco Bay, California. Rev. Geophys. 34(2), 127–168. https://doi.org/10.1029/96RG00986

Cloern, J. E., Jassby, A. D., Thompson, J. K., Hieb, K. A., 2007. A cold phase of the East Pacific triggers new phytoplankton blooms in San Francisco Bay. PNAS. 104(47), 18561–18565. https://doi.org/www.pnas.org/cgi/doi/10.1073/pnas.0706151104

807 Cloern, J. E., Schraga, T. S., Lopez, C. B., 2005. Heat Wave Bring an Unprecedent
808 Red Tide to San Francisco Bay. Ocean Sci. 86(7), 66.
809 https://doi.org/10.1029/2005EO070003
810 Condie, S. A., Oliver, E. C. J., Hallegraeff, G. M., 2019. Environmental drivers of
811 unprecedented *Alexandrium catenella* dinoflagellate blooms off eastern
812 Tasmania, 2012–2018. Harmful Algae. 87, 101628
813 https://doi.org/10.1016/j.hal.2019.101628
814 Corzo, A., Rodríguez-Gálvez, S., Lubian, L., Sangrá, P., Martínez, A., Morillo, J. A.,
815 2005. Spatial distribution of transparent exopolymer particles in the Bransfield
816 Strait, Antarctica. J. Plankton Res. 27(7), 635–646.
817 https://doi.org/10.1093/plankt/fbi038
818 Dagenais-Bellefeuille, S., Morse, D., 2013. Putting the N in dinoflagellates. Front.
819 Microbiol. 4, 369. https://doi.org/10.3389/fmicb.2013.00369
820 Diaz, P. A., Perez-Santos, I., Alvarez, G., Garreaud, R., Pinilla, E., Diaz, M., Sandoval,
821 A., Araya, M., Alvarez, F., Rengel, J., Montero, P., Pizarro, G., Lopez, L., Iritarte,
822 L., Igor, G., Reguera, B. 2021. Multiscale physical background to an exceptional
823 harmful algal bloom of *Dinophysis acuta* in a fjord system. Sci. Total. Environ.
824 773,145621. https://doi.org/10.1016/j.scitotenv.2021.145621
825 Diaz, F., Raimbault, P., 2000. Nitrogen regeneration and dissolved organic nitrogen
826 release during spring in a NW Mediterranean coastal zone (Gulf of Lions):
827 implications for the estimation of new production. Mar. Ecol. Prog. Ser. 197, 51–
828 65. https://www.jstor.org/stable/24855744
829 Diaz, R. J., Rosenberg, R., 2008. Spreading Dead Zones and Consequences for
830 Marine Ecosystems. Science. 321, 926–929.
831 https://doi.org/10.1126/science.1156401

Elbrächter, M., Schnepf, E., 1996. *Gymnodinium chlorophorum*, a new, green, bloom-forming dinoflagellate (Gymnodiniales, Dinophyceae) with a vestigial prasinophyte endosymbiont. *Phycologia.* 35(5), 381-393. https://doi.org/10.2216/i0031-8884-35-5-381.1

Engel, A., 2004. Distribution of transparent exopolymer particles (TEP) in the northeast Atlantic Ocean and their potential significance for aggregation processes. Deep Sea Res. Part I. 51(1), 83–92. https://doi.org/10.1016/j.dsr.2003.09.001

Fuhrman, J. A., 1999. Marine viruses and their biogeochemical and ecological effects. Nature. 399, 541–548. https://doi.org/10.1038/21119

Gárate-Lizárraga, I., Muñetón-Gómez, M., S., Pérez-Cruz, B., Díaz-Ortíz, J., A., 2014. Bloom of *Gonyaulax spinifera* (Dinophyceae: Gonyaulacales) in ensenada de la Paz Lagoon, Gulf of California. CICIMAR Oceánides. 29(1), 11-18. https://doi.org/10.37543/oceanides.v29i1.130

Garvetto, A., Nézan, E., Badis, Y., Bilien, G., Arce, P., Bresnan, E., Gachon, C. M. M., Siano, R., 2018. Novel Widespread Marine Oomycetes Parasitising Diatoms, Including the Toxic Genus *Pseudo-nitzschia*: Genetic, Morphological, and Ecological Characterisation. Front. Microbiol. 9, 1–19. https://doi.org/10.3389/fmicb.2018.02918

Gavalás-Olea, A., Álvarez, S., Riobó, P., Rodríguez, F., Garrido, J. L., Vaz, B., 2016. 19,19′-Diacyloxy Signature: An Atypical Level of Structural Evolution in Carotenoid Pigments. Org. Lett. 18, 4642-4645 https://doi.org/10.1021/acs.orglett.6b02272

Gernez, P., Doxaran, D., Barillé, L., 2017. Shellfish aquaculture from space: potential of Sentinel2 to monitor tide-driven changes in turbidity, chlorophyll concentration and oyster physiological response at the scale of an oyster farm. Front. Mar. Sci. 4, 137. https://doi.org/10.3389/fmars.2017.00137

Giacobbe, M. G., Oliva, F. D. Maimone, G., 1996. Environmental Factors and Seasonal Occurrence of the Dinoflagellate *Alexandrium minutum*, a PSP Potential Producer, in a Mediterranean Lagoon. Estuar. Coast. Shelf Sci. 42, 539–549. https://doi.org/10.1006/ecss.1996.0035

Gilerson, A. A., Gitelson, A. A., Zhou, J., Gurlin, D., Moses, W., Ioannou, I., Ahmed, S. A., 2010. Algorithms for remote estimation of chlorophyll-a in coastal and inland waters using red and near infrared bands. Opt. Express. 18(23), 24109-24125. https://doi.org/10.1364/OE.18.024109

Gitelson, A., 1992. The peak near 700 nm on radiance spectra of algae and water: relationships of its magnitude and position with chlorophyll concentration. Int. J. Remote Sens., 13, 3367-3373. https://doi.org/10.1080/01431169208904125

Glibert, P.M., Wilkerson, F.P., Dugdale, R.C., Raven, J.A., Dupont, C.L., Leavitt, P.R., Parker, A.E., Burkholder, J.M., Kana, T.M., 2016. Pluses and minuses of ammonium and nitrate uptake and assimilation by phytoplankton and implications for productivity and community composition, with emphasis on nitrogen-enriched conditions. Limnol. Oceanogr. 61(1), 165–197. https://doi.org/10.1002/lno.10203

Gobler, C. J., Doherty, O. M., Hattenrath-Lehmann, T. K., Griffith, A. W., Kang, Y., Litaker, R. W., 2017. Ocean warming since 1982 has expanded the niche of toxic algal blooms in the North Atlantic and North Pacific oceans. PNAS. 114(19), 4975–4980. https://doi.org/10.1073/pnas.1619575114

Hall, N. S., Paerl, H. W., Peierls, B. L., Whipple, A. C., Rossignol, K. L., 2013. Effects of climatic variability on phytoplankton community structure and bloom development in the eutrophic, microtidal, New River Estuary, North Carolina, USA. Estuar. Coast. Shelf Sci. 117, 70–82. https://doi.org/10.1016/j.ecss.2012.10.004

Hallegraeff, G., 2010. Ocean climate change, phytoplankton community responses,

and harmful algal blooms: a formidable predictive challenge. J. Phycol. 46, 220–235. https://doi.org/10.1111/j.1529-8817.2010.00815.x

Hansen, G., Botes, L., De Salas, M., 2007. Ultrastructure and large subunit rDNA sequences of *Lepidodinium viride* reveal a close relationship to *Lepidodinium chlorophorum* comb. nov. (= *Gymnodinium chlorophorum*). Phycological Res. 55, 25–41. https://doi.org/10.1111/j.1440-1835.2006.00442.x

Hansen, G., Moestrup, Ø., 2005. Flagellar apparatus and nuclear chambers of the green dinoflagellate *Gymnodinium chlorophorum*. Phycol. Res. 53(2), 169–181. https://doi.org/10.1111/j.1440- 183.2005.00383.x

Harmel, T., Chami, M., Tormos, T., Reynaud, N., Danis, P. A., 2018. Sunglint correction of the Multi-Spectral Instrument (MSI)-SENTINEL-2 imagery over inland and sea waters from SWIR bands. Remote Sens. Environ. 204, 308-321. https://doi.org/10.1016/j.rse.2017.10.022

Hasui, M., Matsuda, M., Okutani, K., Shigeta, S., 1995. *In vitro* antiviral activities of sulfated polysaccharides from a marine microalga (*Cochlodinium polykrikoides*) against human immunodeficiency virus and other enveloped viruses. Int. J. Biol. Macromol. 17, 293-297. https://doi.org/10.1016/0141-8130(95)98157-T

Herreid, C. F., 1980. Hypoxia in invertebrates. Comp. Biochem. Physiol. 67, 311–320. https://doi.org/10.1016/S0300-9629(80)80002-8

Hicks, D. W., McMahon, R. F., 2002. Respiratory responses to temperature and hypoxia in the nonindigenous Brown Mussel, *Perna perna* (Bivalvia: Mytilidae), from the Gulf of Mexico. J. Exp. Mar. Biol. Ecol. 277, 61–78. https://doi.org/https://doi.org/10.1016/S0022-0981(02)00276-9

Honsell, G., Talarico, L., Cabrini, M., 1988. Interesting ultrastructural features of a green dinoflagellate, G. Bot. Ital. 122, 76–78.

Honsell, G., Talarico, L., 2004. *Gymnodinium chlorophorum* (Dinophyceae) in the Adriatic Sea: Electron microscopical observations. Botanica Marina. 47, 152–166. https://doi.org/10.1515/BOT.2004.016

Iriarte, J. L., Quiñones, R. A., González, R. R., 2005. Relationship between biomass and enzymatic activity of a bloom-forming dinoflagellate (Dinophyceae) in southern Chile (41° S): a field approach. J. Plankton Res. 27(2), 159–166. https://doi.org/10.1093/plankt/fbh167

Iverson, R. L., Curl, H. C., O'Connors, H. B., Kirk, J. D., Zakar, K., 1974. Summer phytoplankton blooms in Auke Bay, Alaska, driven by wind mixing of the water column. Limnol. Oceanogr. 19(2), 271–278. https://doi.org/10.4319/lo.1974.19.2.0271

Jackson, C., Knoll, A. H., Chan, C. X., Verbruggen, H., 2018. Plastid phylogenomics with broad taxon sampling further elucidates the distinct evolutionary origins and timing of secondary green plastids. Sci. Rep. 8, 1523. https://doi.org/10.1038/s41598-017-18805-w

Jeong, H. J., Yoo, Y. D., Kang, N. S., Rho, J. R., Seong, K. A., Park, J. W., Nam, G. S., Yih, W., 2010. Ecology of *Gymnodinium aureolum.* I. Feeding in western Korean waters. Aquat. Microb. Ecol. 59, 239–255. https://doi.org/10.3354/ame01394

Kamikawa, R., Tanifuji, G., Kawachi, M., Miyashita, H., Hashimoto, T., Inagaki, Y., 2015. Plastid genome-based phylogeny pinpointed the origin of the green-colored plastid in the dinoflagellate *Lepidodinium chlorophorum*. Genome Biol. Evol. 7(4), 1133-1140. https://doi.org/10.1093/gbe/evv060

Karasiewicz, S., Chapelle, A., Bacher, C., Soudant, D., 2020. Harmful algae niche responses to environmental and community variation along the French coast.

Harmful Algae. 93, 101785. https://doi.org/10.1016/j.hal.2020.101785

Kononen, K., Huttunen, M., Hällfors, S., Gentien, P., Lunven, M., Huttula, T., Laanemets, J., Lilover, M., Pavelson, J., Stips, A., 2003. Development of a deep chlorophyll maximum of *Heterocapsa triquetra* Ehrenb. at the entrance to the Gulf of Finland. Limnol. Oceanogr. 48(2), 594–607. https://doi.org/10.4319/lo.2003.48.2.0594

Lavigne, H., Van der Zande, D., Ruddick, K., Dos Santos, J. C., Gohin, F., Brotas, V., Kratzer, S., 2021. Quality-control tests for OC4, OC5 and NIR-red satellite chlorophyll-a algorithms applied to coastal waters. Remote Sens. of Environ. 255, 112237. https://doi.org/10.1016/j.rse.2020.112237

Lazure, P., Garnier, V., Dumas, F., Herry, C., Chifflet, M., 2009. Development of a hydrodynamic model of the Bay of Biscay. Validation of hydrology. Cont. Shelf Res. 29, 985–997. https://doi.org/10.1016/j.csr.2008.12.017

Lazure, P., Jégou, A. M., 1998. 3D modelling of seasonal evolution of Loire and Gironde plumes on Biscay Bay continental shelf. Oceanologica Acta. 21(2), 165–177. https://doi.org/10.1016/S0399-1784(98)80006-6

Lazure, P., Salomon, J. C., 1991. Coupled 2-D and 3-D modelling of coastal hydrodynamics. Oceanologica Acta. 14(2), 173–180.

Lee, Z. P., Du, K. P., Arnone, R., 2005. A model for the diffuse attenuation coefficient of downwelling irradiance. J. Geophys. Res. Oceans. 110(C2). https://doi.org/10.1029/2004JC002275

Lips, U., Lips, I., Liblik, T., Kuvaldina, N., 2010. Processes responsible for the formation and maintenance of sub-surface chlorophyll maxima in the Gulf of Finland. Estuar. Coast. Shelf Sci. 88, 339–349. https://doi.org/10.1016/j.ecss.2010.04.015

Liu, K., Ng, H. Y. T., Zhang, S., Liu, H., 2021. Effects of temperature on a mixotrophic

957 dinoflagellate (*Lepidodinium* sp.) under different nutritional strategies. Mar. Ecol.
958 Prog. Ser. 678, 37-49. https://doi.org/10.3354/meps13865
959 Lucas, L. V., Koseff, J. R., Monismith, S. G., Cloern, J. E., Thompson, J. K., 1999a.
960 Processes governing phytoplankton blooms in estuaries. II: The role of horizontal
961 transport. Mar. Ecol. Prog. Ser. 187, 17-30.
962 Lucas, L. V., Koseff, J. R., Cloern, J. E., Monismith, S. G., Thompson, J. K., 1999b.
963 Processes governing phytoplankton blooms in estuaries. I: The local production-
964 loss balance. Mar. Ecol. Prog. Ser. 187, 1-15.
965 Lyons, M.M., Lau, Y.T., Carden, W.E., Ward, J.E., Roberts, S.B., Smolowitz, R.,
966 Vallino, J., Allam, B., 2007. Characteristics of marine aggregates in shallow-water
967 ecosystems: Implications for disease ecology. EcoHealth 4(4), 406–420.
968 https://doi.org/10.1007/s10393-007-0134-0
969 Main-Knorn, M., Pflug, B., Louis, J., Debaecker, V., Müller-Wilm, U., Gascon, F., 2017.
970 Sen2Cor for Sentinel-2. SPIE Remote Sensing. SPIE, 12.
971 https://doi.org/10.1117/12.2278218.
972 Mandal, S. K., Singh, R. P., Patel, V., 2011. Isolation and Characterization of
973 Exopolysaccharide Secreted by a Toxic Dinoflagellate, *Amphidinium carterae*
974 Hulburt 1957 and Its Probable Role in Harmful Algal Blooms (HABs). Microbial
975 Ecology. 62, 518–527. https://doi.org/10.1007/s00248-011-9852-5
976 Margalef, R., 1978. Life-forms of phytoplankton as survival alternatives in an unstable
977 environment. Oceanologica Acta, 1(4), 493–509.
978 Mari, X., Passow, U., Migon, C., Burd, A. B., Legendre, L., 2017. Transparent
979 exopolymer particles: Effects on carbon cycling in the ocean. Prog. Oceanogr.
980 151, 13-37. https://doi.org/10.1016/j.pocean.2016.11.002
981 Matsumoto, T., Shinozaki, F., Chikuni, T., Yabuki, A., Takishita, K., Kawachi, M.,

Nakayama, T., Inouye, I., Hashimoto, T., Inagaki, Y., 2011. Green-colored Plastids in the Dinoflagellate Genus *Lepidodinium* are of Core Chlorophyte Origin. Protist. 162, 268-276. https://doi.org/10.1016/j.protis.2010.07.001

McCarthy, P. M., 2013. Census of Australian Marine Dinoflagellates. Australian Biological Resources Study, Canberra. http://www.anbg.gov.au/abrs/Dinoflagellates/index_Dino.html [version 11 July 2013].

Ménesguen, A., Dussauze, M., 2015. Détermination des “bassins récepteurs” marins des principaux fleuves français de la façade Manche-Atlantique, et de leurs rôles respectifs dans l’eutrophisation phytoplanctonique des masses d’eau DCE et des sous-régions DCSMM. Nantes, France. https://archimer.ifremer.fr/doc/00333/44422/

Ménesguen, A., Desmit, X., Dulière, V., Lacroix, G., Thouvenin, B., Thieu, V., Dussauze, M., 2018. How to avoid eutrophication in coastal seas? A new approach to derive river-specific combined nitrate and phosphate maximum concentrations. Sci. Total Environ. 628–629, 400–414. https://doi.org/10.1016/j.scitotenv.2018.02.025

Ng, W.H.A., Liu, H., Zhang, S., 2017. Diel variation of grazing of the dinoflagellate *Lepidodinium* sp. and ciliate Euplotes sp. on algal prey: The effect of prey cell properties. J. Plankton Res. 39(3), 450-462. https://doi.org/10.1093/plankt/fbx020

Nielsen, T. G., Kiørboe, T., Bjørnsen, P. K., 1990. Effects of a *Chrysochromulina polylepis* subsurface bloom on the planktonic community. Mar. Ecol. Prog. Ser. 62(1/2), 21–35. https://doi.org/10.3354/meps062021

Odebrecht, C., Abreu, P. C., Carstensen, J., 2015. Retention time generates short-term phytoplankton blooms in a shallow microtidal subtropical estuary. Estuar.

Coast. Shelf Sci. 162, 35–44. https://doi.org/10.1016/j.ecss.2015.03.004

O'Reilly, J. E., Maritorena, S., Mitchell, B. G., Siegel, D. A., Carder, K. L., Garver, S. A., Kahru, M., McClain, C. 1998. Ocean color chlorophyll algorithm for SeaWiFS. J. Geophys. Res. 103, 24937–24953.

Ortega-Retuerta, E., Reche, I., Pulido-Villena, E., Agustí, S., Duarte, C. M., 2009. Uncoupled distributions of transparent exopolymer particles (TEP) and dissolved carbohydrates in the Southern Ocean. Mar. Chem. 115, 59–65. https://doi.org/10.1016/j.marchem.2009.06.004

Ortega-Retuerta, E., Duarte, C. M., Reche, I., 2010. Significance of bacterial activity for the distribution and dynamics of transparent exopolymer particles in the Mediterranean Sea. Microb. Ecol. 59, 808–818. https://doi.org/10.1007/s00248-010-9640-7

Paerl, H. W., 1997. Coastal eutrophication and harmful algal blooms: Importance of atmospheric deposition and groundwater as "new" nitrogen and other nutrient sources. Limnol. Oceanogr. 42(5), 1154–1165. https://doi.org/10.4319/lo.1997.42.5_part_2.1154

Paulmier, G., Berland, B., Billard, C., Nezan, E., 1995. *Gyrodinium corsicum* nov. sp. (Gymnodiniales, Dinophycees), organisme responsable d′une «eau Verte» dans l′Etang marin de Diana (Corse), en Avril 1994. Cryptogam. Algol. 16, 77–94.

Passow, U., 2002. Transparent exopolymer particles (TEP) in aquatic environments. Prog. Oceanogr. 55, 287-333. https://doi.org/10.1016/S0079-6611(02)00138-6

Passow U., Alldredge A. L., 1995. A dye-binding assay for the spectrophotometric measurement of transparent exopolymer particles (TEP). Limnol. Oceanogr. 40(7), 1326–1335. https://doi.org/10.4319/lo.1995.40.7.1326

Passow, U., Engel, A., 2001. Carbon and nitrogen content of transparent exopolymer

particles (TEP) in relation to their Alcian Blue adsorption. Mar. Ecol. Prog. Ser. 219, 1–10. https://doi.org/10.3354/meps219001

Passow, U., Shipe, R. F., Murray, A., Pak, D. K., Brzezinski, M. A., Alldredge, A. L., 2001. The origin of transparent exopolymer particles (TEP) and their role in the sedimentation of particulate matter. Cont. Shelf Res. 21, 327-346.

Peierls, B. L., Hall, N. S., Paerl, H. W., 2012. Non-monotonic responses of phytoplankton biomass accumulation to hydrologic variability: A comparison of two coastal plain North Carolina Estuaries. Estuaries Coast. 35, 1376–1392. https://doi.org/10.1007/s12237-012-9547-2

Petersen, J. K., Nielsen, T. G., van Duren, L., Maar, M., 2008. Depletion of plankton in a raft culture of *Mytilus galloprovincialis* in Ría de Vigo, NW Spain. I. Phytoplankton. Aquat. Biol. 4, 113–125. https://doi.org/10.3354/ab00124

Planque, B., Lazure, P., Jégou, A. M., 2004. Detecting hydrological landscapes over the Bay of Biscay continental shelf in spring. Clim. Res. 28, 41–52. https://doi.org/10.3354/cr028041

Prieto, L., Navarro, G., Cózar, A., Echevarría, F., García, C. M., 2006. Distribution of TEP in the euphotic and upper mesopelagic zones of the southern Iberian coasts. Deep Sea Res. II. 53, 1314–1328. https://doi.org/10.1016/j.dsr2.2006.03.009

Puillat, I., Lazure, P., Jégou, A. M., Lampert, L., Miller, P., 2004. Hydrographical variability on the French continental shelf in the Bay of Biscay, during the 1990s. Cont. Shelf Res. 24, 1143–1163. https://doi.org/10.1016/j.csr.2004.02.008

Puillat, I., Lazure, P., Jégou, A. M., Lampert, L., Miller, P., 2006. Mesoscale hydrological variability induced by northwesterly wind on the French continental shelf of the Bay of Biscay. Scientia Marina, 15–26. https://doi.org/10.3989/scimar.2006.70s115

Qi, L., Hu, C., 2021. To what extent can *Ulva* and *Sargassum* be detected and separated in satellite imagery? Harmful Algae, 103, 102001. https://doi.org/10.1016/j.hal.2021.102001

Quevedo, M., Gonzalez-Quiros, R., Anadon, R., 1999. Evidence of heavy predation by *Noctiluca scintillans* on *Acartia clausi* (Copepoda) eggs off the central Cantabrian coast (NW Spain). Oceanologica Acta. 22(1), 127–131. https://doi.org/10.1016/S0399-1784(99)80039-5

Raimbault, P., Pouvesle, W., Diaz, F., Garcia, N., Sempere, R., 1999. Wet-oxidation and automated colorimetry for simultaneous determination of organic carbon, nitrogen and phosphorus dissolved in seawater. Mar. Chem. 66, 161-169. https://doi.org/10.1016/S0304-4203(99)00038-9

Ratmaya, W., Soudant, D., Salmon-Monviola, J., Plus, M., Cochennec-Laureau, N., Goubert, E., Andrieux-Loyer, F., Barillé, L., Souchu, P., 2019. Reduced phosphorus loads from the Loire and Vilaine rivers were accompanied by increasing eutrophication in the Vilaine Bay (south Brittany, France). Biogeosciences. 16, 1361–1380. https://doi.org/10.5194/bg-16-1361-2019

R Core Team: A Language and Environment for Statistical Computing. 2019. R Foundation for Statistical Computing, Vienna. https://www.R-project.org

Redfield, A. C., 1958. The biological control of chemical factors in the environment. Am. Sci. 46(3), 205-221. https://www.jstor.org/stable/27827150

[dataset] REPHY - French Observation and Monitoring program for Phytoplankton and Hydrology in coastal waters. 2021. REPHY dataset - French Observation and Monitoring program for Phytoplankton and Hydrology in coastal waters. Metropolitan data. SEANOE. https://doi.org/10.17882/47248

[dataset] Retho, M., Quemener, L., Le Gall, C., Repecaud, M., Souchu, P., Gabellec,

R., Manach S., 2020. MOLIT Vilaine data and metadata from Coriolis Data Centre. SEANOE. https://doi.org/10.17882/46529

Richardson, K., Visser, A. W., Pedersen, F. B., 2000. Subsurface phytoplankton blooms fuel pelagic production in the North Sea. J. Plankton Res. 22(9), 1663–1671. https://doi.org/10.1093/plankt/22.9.1663

Rodríguez-Benito, C. V., Navarro, G., Caballero, I., 2020. Using Copernicus Sentinel-2 and Sentinel-3 data to monitor harmful algal blooms in Southern Chile during the COVID-19 lockdown. Mar. Pollut. Bull. 161, 111722. https://doi.org/10.1016/j.marpolbul.2020.111722

Rosenberg, R., Hellman, B., Johansson, B., 1991. Hypoxic tolerance of marine benthic fauna. Mar. Ecol. Prog. Ser. 79, 127–131. https://doi.org/10.3354/meps079127

Rossignol-Strick, M., 1985. A marine anoxic event on the Brittany coast, July 1982. J. Coast. Res. 1(1), 11-20

Roux, P., Siano, R., Collin, K., Bilien, G., Sinquin, C., Marchand, L., Zykwinska, A., Delbarre-Ladrat, C., Schapira, M., 2021. Bacteria enhance the production of extracellular polymeric substances by the green dinoflagellate *Lepidodinium chlorophorum*. Sci. Rep. 11, 4795. https://doi.org/10.1038/s41598-021-84253-2

Schapira, M., McQuaid, C. D., Froneman, P. W., 2012a. Metabolism of free-living and particle-associated prokaryotes: Consequences for carbon flux around a Southern Ocean archipelago. J. Mar. Syst. 90, 58–66. https://doi.org/10.1016/j.jmarsys.2011.08.009

Schapira, M., McQuaid, C. D., Froneman, P. W., 2012b. Free-living and particle-associated prokaryote metabolism in giant kelp forests: Implications for carbon flux in a sub-Antarctic coastal area. Estuar. Coast. Shelf Sci. 106, 69–79. https://doi.org/10.1016/j.ecss.2012.04.031

1107 Schlitzer, R., 2020. Ocean Data View ⟨http://odv.awi.de⟩

1108 Serre-Fredj, L., Jacqueline, F., Navon, M., Izabel, G., Chasselin, L., Jolly, O.,
1109 Repecaud, M., Claquin, P., 2021. Coupling high frequency monitoring and
1110 bioassay experiments to investigate a harmful algal bloom in the Bay of Seine
1111 (French-English Channel). Mar. Pollut. Bull. 168, 112387.
1112 https://doi.org/10.1016/j.marpolbul.2021.112387

1113 Shapiro, K., Krusor, C., Mazzillo, F.F.M., Conrad, P.A., Largier, J.L., Mazet, J.A.K.,
1114 Silver, M.W., 2014. Aquatic polymers can drive pathogen transmission in coastal
1115 ecosystems. Proc. Royal Soc. B 281(1795), 1-9.
1116 https://doi.org/10.1098/rspb.2014.1287

1117 Shikata, T., Nagasoe, S., Matsubara, T., Yoshikawa, S., Yamasaki, Y., Shimasaki, Y.,
1118 Oshima, Y., Jenkinson, I. R., Honjo, T., 2008. Factors influencing the initiation of
1119 blooms of the raphidophyte *Heterosigma akashiwo* and the diatom *Skeletonema*
1120 *costatum* in a port in Japan. Limnol. Oceanogr. 53(6), 2503–2518.
1121 https://doi.org/10.2307/40058340

1122 Siano, R., Alves-De-Souza, C., Foulon, E., Bendif, E. M., Simon, N., Guillou, L., Not,
1123 F., 2011. Distribution and host diversity of Amoebophryidae parasites across
1124 oligotrophic waters of the Mediterranean Sea. Biogeosciences. 8, 267–278.
1125 https://doi.org/10.5194/bg-8-267-2011

1126 Siano, R., Chapelle, A., Antoine, V., Michel-Guillou, E., Rigaut-Jalabert, F., Guillou, L.,
1127 Hégaret, H., Leynaert, A., Curd, A., 2020. Citizen participation in monitoring
1128 phytoplankton seawater discolorations. Mar. Policy. 117, 103039.
1129 https://doi.org/10.1016/j.marpol.2018.01.022

1130 Simon, M., Grossart, H.P., Schweitzer, B., Ploug, H., 2002. Microbial ecology of
1131 organic aggregates in aquatic ecosystems. Aquat. Microb. Ecol. 28(2), 175–211.

https://doi.org/10.3354/ame028175

Smayda, T.J., 2002a. Turbulence, watermass stratification and harmful algal blooms: an alternative view and frontal zones as “pelagic seed banks.” Harmful Algae. 1, 95–112. https://doi.org/10.1016/S1568-9883(02)00010-0

Smayda, T.J., 2002b. Adaptative Ecology, Growth Strategies and the Global Bloom Expansion of Dinoflagellates. J. Oceanogr. 58, 281-294. https://doi.org/10.1023/A:1015861725470

Sobral, P., Widdows, J., 1997. Influence of hypoxia and anoxia on the physiological responses of the clam *Ruditapes decussatus* from southern Portugal. Mar. Biol. 127, 455–461. https://doi.org/10.1007/s002270050033

Sourisseau, M., Jegou, K., Lunven, M., Quere, J., Gohin, F., Bryere, P., 2016. Distribution and dynamics of two species of Dinophyceae producing high biomass blooms over the French Atlantic Shelf. Harmful Algae. 53, 53-63. https://doi.org/10.1016/j.hal.2015.11.016

Sournia, A., Belin, C., Billard, C., Erard-Le Denn, E., Fresnel, J., Lassus, P., Pastoureau, A., Soulard, R., 1992. The repetitive and expanding occurrence of green, bloom-forming dinoflagellate (Dinophyceae) on the coasts of France. Cryptogam. Algol. 13(1), 1–13.

Steinmetz, F., Deschamps, P. Y., Ramon, D., 2011. Atmospheric correction in presence of sun glint: application to MERIS. Opt. express. 19(10), 9783-9800. https://doi.org/10.1364/OE.19.009783

Suttle, C. A., 2007. Marine viruses - Major players in the global ecosystem. Nat. Rev. Microbiol. 5, 801–812. https://doi.org/10.1038/nrmicro1750

Thomas, Y., Pouvreau, S., Alunno-Bruscia, M., Barillé, L., Gohin, F., Bryere, P., Gernez, P., 2016. Global change and climate-driven invasion of the Pacific oyster

(*Crassostrea gigas*) along European coasts: a bioenergetics modelling approach. J. Biogeogr. 43(3), 568–579. https://doi.org/10.1111/jbi.12665

Traini, C., Proust, J. N., Menier, D., Mathew, M. J., 2015. Distinguishing natural evolution and human impact on estuarine morpho-sedimentary development: A case study from the Vilaine Estuary, France. Estuar. Coast. Shelf Sci. 163, 143–155. https://doi.org/10.1016/j.ecss.2015.06.025

Utermöhl, H., 1958. Zur vervollkommnung der quantitativen phytoplankton methodik. Mitteilungen-Internationale Vereiningung fur Limnologie. 9, 1-38

Velo-Suárez, L., Reguera, B., Garcés, E., Wyatt, T., 2009. Vertical distribution of division rates in coastal dinoflagellate *Dinophysis* spp. populations: implications for modelling. Mar. Ecol. Prog. Ser. 385, 87–96. https://doi.org/10.3354/meps08014

Yamamoto, K., Tsujimura, H., Nakajima, M., Harrison, P. J., 2013. Flushing rate and salinity may control the blooms of the toxic dinoflagellate *Alexandrium tamarense* in a river/estuary in Osaka Bay, Japan. J. Oceanogr. 69, 727–736. https://doi.org/10.1007/s10872-013-0203-7

Yim, J. H., Kim, S. J., Ahn, S. H., Lee, H. K., 2007. Characterization of a novel bioflocculant, p-KG03, from a marine dinoflagellate, *Gyrodinium impudicum* KG03. Bioresour. Technol. 98(2), 361–367. https://doi.org/10.1016/j.biortech.2005.12.021

Zeng, C., Binding, C., 2019. The effect of mineral sediments on satellite chlorophyll-a retrievals from line-height algorithms using red and near-infrared bands. Remote Sens. 11(19), 2306. https://doi.org/10.3390/rs11192306

Zhang, W., Dong, Z., Zhang, C., Sun, X., Hou, C., Liu, Y., Wang, L., Ma, Y., Zhao, J., 2020. Effects of physical-biochemical coupling processes on the *Noctiluca*

*scintillans* and *Mesodinium* red tides in October 2019 in the Yantai nearshore, China. Mar. Pollut. Bull. 160, 111609. https://doi.org/10.1016/j.marpolbul.2020.111609

Zingone, A., Enevoldsen, O. H., 2000. The diversity of harmful algal blooms: a challenge for science and management. Ocean Coast. Manag. 43, 725-748. https://doi.org/10.1016/S0964-5691(00)00056-9

## LEGENDS

**Figure 1.** Location of the three sampling stations of the Vilaine Bay (Nord Dumet, Ouest Loscolo) and Quiberon Bay (Men er Roue) monitored in 2019 in Southern Brittany coast (NE Atlantic, France).

**Figure 2.** Variations in hydrological parameters associated with phytoplankton recorded in 2019 at the three sampling stations of the Vilaine Bay (Ouest Loscolo, Nord Dumet) and Quiberon Bay (Men er Roue). Abundances of *L. chlorophorum* (cells $L^{-1}$) are represented in logarithmic scale. Solid lines represent values measured at the subsurface, and dashed lines represent values obtained at the water-sediment interface (WSI). Values measured at the Fmax depth are not included in the figure and are presented in Table 1.

**Figure 3**. (**A–F**) Examples of Sentinel-2 images (11, 16, and 21 July 2019) acquired during the green seawater discoloration in summer 2019. Upper panel: RGB images; lower panel: the reflectance ratio $R_{rs}(705)/R_{rs}(665)$ is shown as a proxy of chlorophyll *a* concentration. (**G**) Location of regular stations in the Vilaine Bay, as well as the additional stations specifically sampled during the bloom field experiment on July 9, 2019. The map shows a qualitative estimate of the chlorophyll *a* concentration estimated from the Landsat-8 image acquired 9 July 2019. (**H**) Field picture of green seawater discoloration caused by *Lepidodinium chlorophorum*.

**Figure 4**. Relative abundances (%) of the main microphytoplankton genera or species observed inside (St1, St2, St3) and outside (St4, St5, St6) the green seawater discoloration (**A**) at the subsurface and (**B**) water-sediment interface.

**Figure 5**. Spatial distribution of biological and physicochemical parameters: (**A**) *L. chlorophorum* concentrations, (**B**) temperature, (**C**) salinity, (**D**) silicates (DSi), (**E**) ammonium ($NH_4$), (**F**) phosphates (DIP), (**G**) dissolved organic nitrogen (DON), and (**H**) transparent exopolymer particles (TEP), measured inside (St1, St2, St3) and outside (St4, St5, St6) the bloom (Ocean Data View, 5.3.0).

**Table 1.** Abundances of *L. chlorophorum* recorded at the fluorescence maximum depth (Fmax) in 2019 at Nord Dumet, Ouest Loscolo and Men er Roue stations.

| Station | Date | *L. chlorophorum* (cells $L^{-1}$) | Depth (m) |
|---|---|---|---|
| Nord Dumet | 11 June 2019 | $1.3 \times 10^3$ | 6.5 |
| Nord Dumet | 08 July 2019 | $9.0 \times 10^2$ | 13.0 |
| Nord Dumet | 22 July 2019 | $2.6 \times 10^5$ | 10.5 |
| Nord Dumet | 09 September 2019 | 0 | 11.0 |
| Ouest Loscolo | 09 September 2019 | 0 | 6.7 |
| Men er Roue | 06 August 2019 | $5.0 \times 10^5$ | 5.6 |

**Table 2.** Satellite-derived estimation of bloom surface using Sentinel-2 images (NA = Bloom visible; surface not computed due to cloud cover), the tidal phase, and the water height difference compared to low tide were obtained from the data of the Oceanographic and Hydrological Service of the French National Navy (SHOM).

| Date | Bloom surface ($km^2$) | Tide type | Water height difference compared to low tide (m) | Tidal phase |
|---|---|---|---|---|
| 16 June 2019 | NA | spring | 1.72 | flow tide |
| 21 June 2019 | 2.67 (+/- 1.08) | neap | 0.44 | ebb tide |
| 26 June 2019 | 12.95 (+/- 1.66) | neap | 1.89 | high tide |
| 01 July 2019 | NA | spring | 1.72 | flow tide |
| 06 July 2019 | 11.12 (+/- 4.75) | spring | 0.61 | ebb tide |
| 11 July 2019 | 2.46 (+/- 1.14) | neap | 3.00 | high tide |
| 16 July 2019 | 2.37 (+/- 0.98) | neap | 1.01 | flow tide |
| 21 July 2019 | 2.91 (+/- 1.03) | neap | 0.57 | ebb tide |

NB: In the shallow waters (depth < 4 m) where the bloom occurred, vertically-resolved field sampling documented high abundance of *L. chlorophorum* from the surface down to about 2 m (Fig. 5A), which is roughly similar to the penetration depth of satellite measurement (about 2.6 m). Furthermore, during that period, samples from the offshore stations (i.e., Nord Dumet and Men er Roue, Fig. S1) did not show significant amounts of *L. chlorophorum* at depths. It is therefore likely that Sentinel-2 detected most of the bloom biomass.

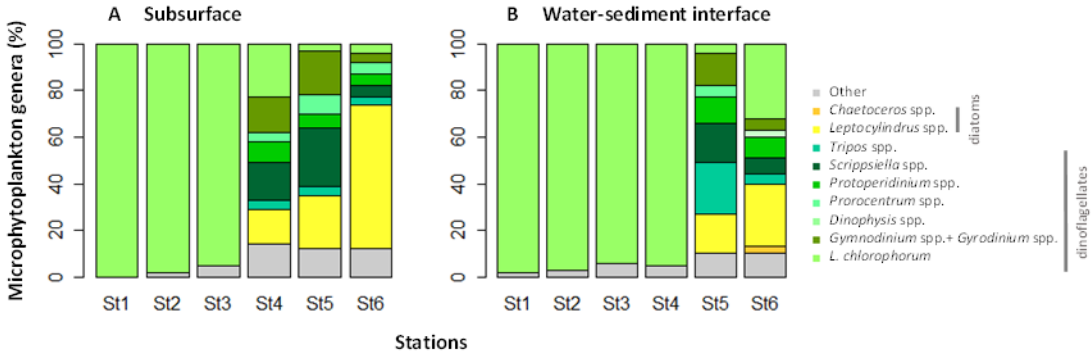

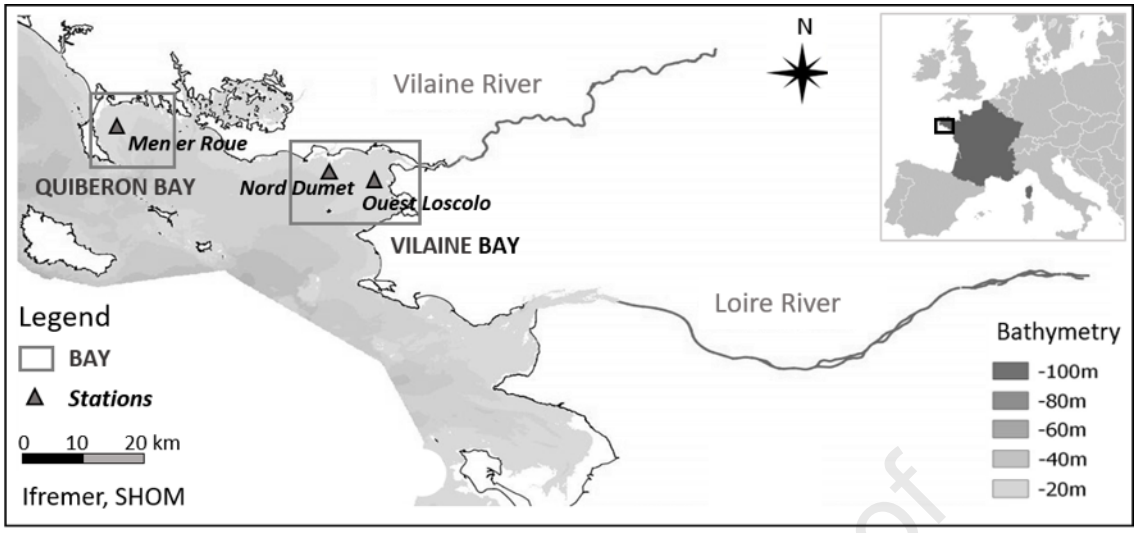

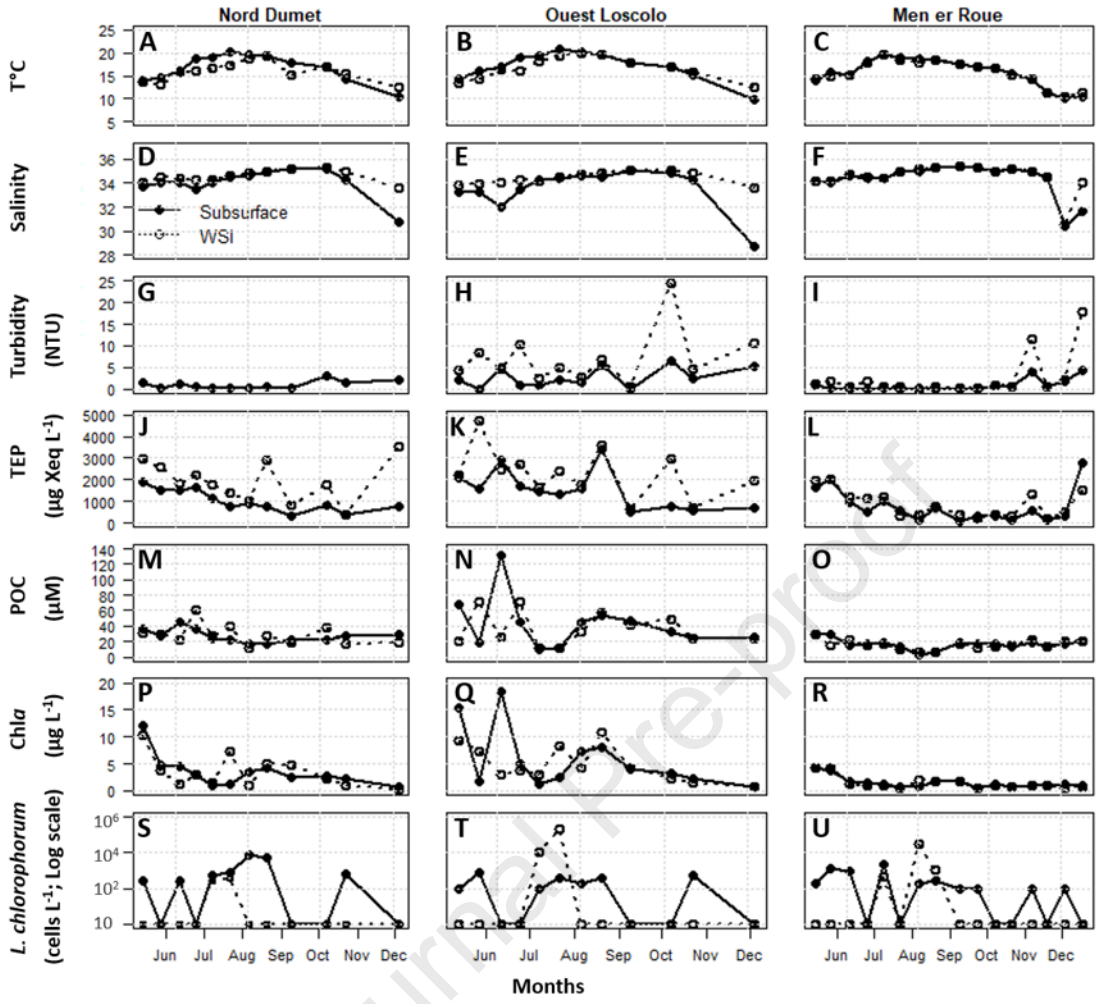

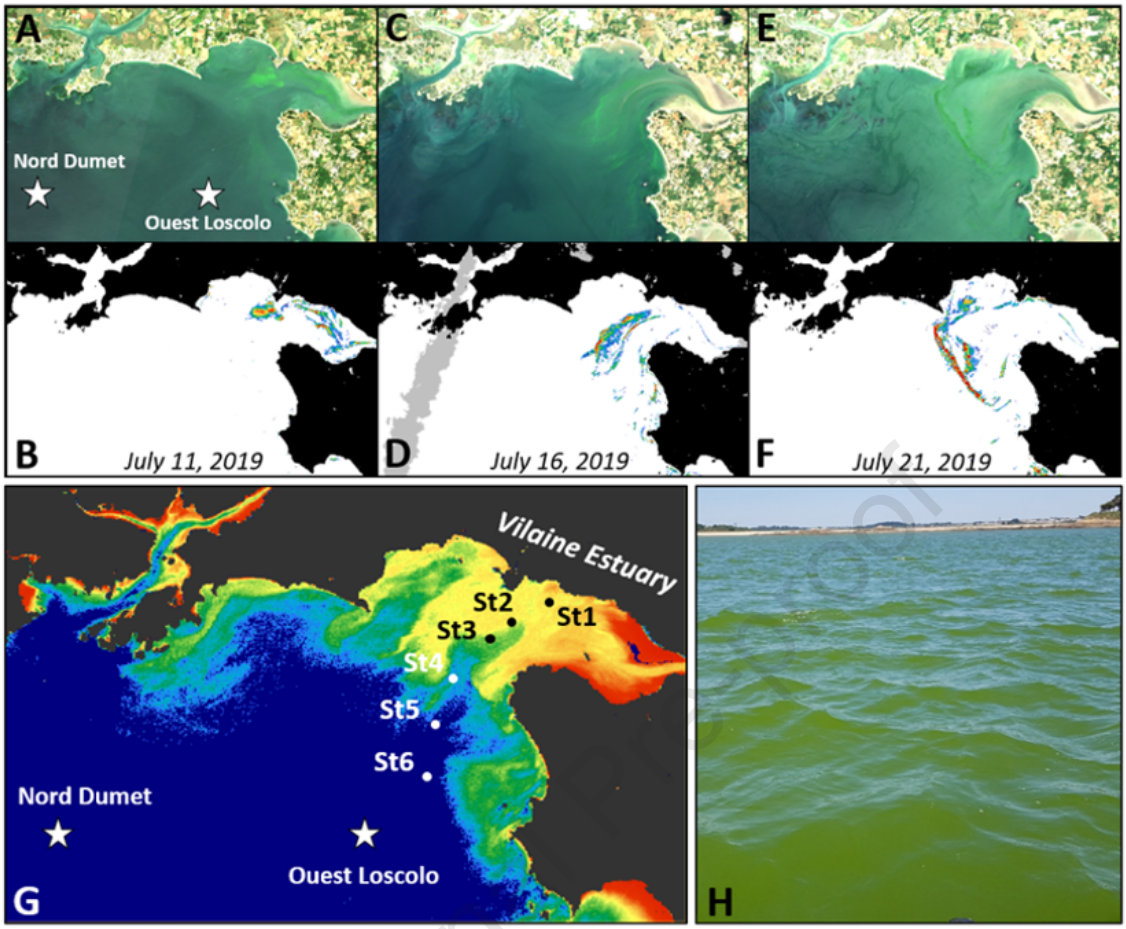

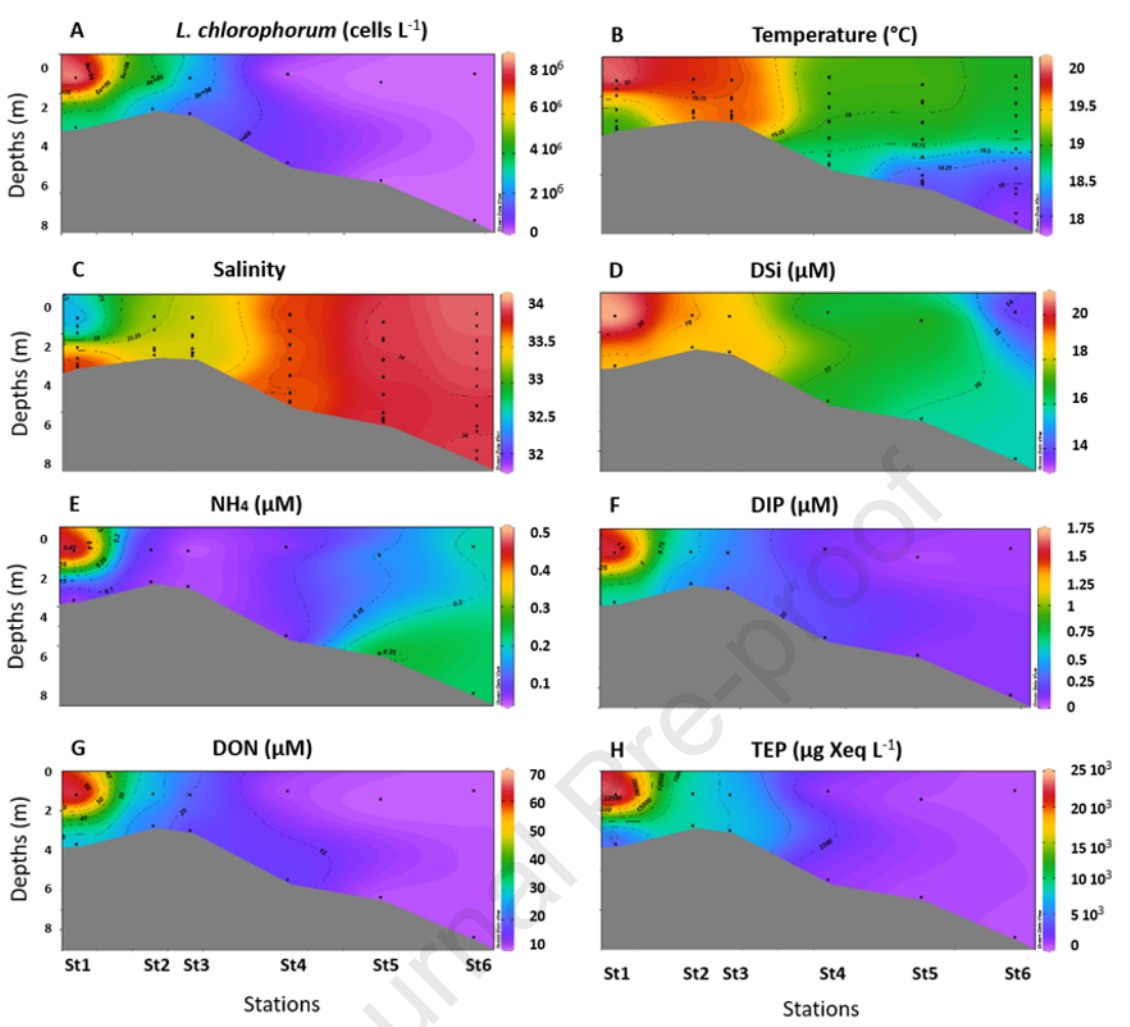

## Highlights

- *Lepidodinium chlorophorum* occurred from May to November in southern Brittany.
- Water column stratification could favour *L*. *chlorophorum* blooms.
- High-resolution (5 days, 20 m) satellite observation made possible to document the bloom surface extent and to highlight the influence of tides on the spatial distribution of *L*. *chlorophorum*.
- High transparent exopolymer particles (TEP) concentrations are measured inside a bloom. Bacterial remineralisation might sustain bloom development for more than one month and cause hypoxia, likely contributing to bivalve mortality.

**Declaration of interests**

☒The authors declare that they have no known competing financial interests or personal relationships that could have appeared to influence the work reported in this paper.

☐The authors declare the following financial interests/personal relationships which may be considered as potential competing interests: